On the stability relationships between tidal asymmetry and morphologies of tidal basins and estuaries

Zeng Zhou[1,2], Giovanni Coco[2], Ian Townend[3,5], Zheng Gong*[1,5], Zhengbing Wang[4], and Changkuan Zhang[5]

[1]Jiangsu Key Laboratory of Coast Ocean Resources Development and Environment Security, Hohai University, Nanjing, China

[2]School of Environment, University of Auckland, New Zealand

[3]Ocean and Earth Sciences, University of Southampton, UK

[4]Faculty of Civil Engineering and Geosciences, Delft University of Technology, Delft, Netherlands

[5]College of Harbour, Coastal and Offshore Engineering, Hohai University, Nanjing,China

Abstract

Simple stability relationships are practically useful to provide a rapid assessment of coastal and estuarine landforms in response to human interventions and long-term climate change. In this contribution, we review a variety of simple stability relationships which are based on the analysis of tidal asymmetry (shortened to "TA"). Most of the existing TA-based stability relationships are derived using the one-dimensional tidal flow equations assuming a certain regular shape of the tidal channel cross-sections. To facilitate analytical solutions, specific assumptions inevitably need to be made e.g. by linearising the friction term and dropping some negligible terms in the tidal flow equations. We find that three major types of TA-based stability relationships have been proposed between three non-dimensional channel geometric ratios (represented by the ratio of channel widths, ratio of wet surface areas and ratio of storage volumes) and the tide-related parameter a/h (i.e.

*Corresponding author. Email: gongzheng@hhu.edu.cn

the ratio between tidal amplitude and mean water depth). Based on established geometric relations, we use these non-dimensional ratios to re-state the existing relationships so that they are directly comparable. Available datasets are further extended to examine the utility of these TA-based relationships. Although a certain agreement is shown for these relationships, we also observe a large scatter of data points which are collected in different types of landscape, hydrodynamic and sedimentologic settings over the world. We discuss in detail the potential reasons for this large scatter and subsequently elaborate on the limited applicability of the various TA-based stability relationships for practical use. We highlight the need to delve further into what constitutes equilibrium and what is needed to develop more robust measures to determine the morphological state of these systems.

Keywords: tidal basins, estuarine morphologies, tidal asymmetry, stability relationships

1 Introduction

Tidal basins and estuaries are highly complex coastal systems that have evolved rapidly during the Holocene transgression and have been shaped by various interactions between hydrodynamics, geomorphology, biological activities, climate variations and human interventions. Nonetheless, analyses of field observations indicate that the gross characteristics of these complicated landscapes when they are morphologically stable (i.e. at or near to equilibrium) can be satisfactorily described by relationships that are fairly simple (e.g. Jarrett, 1976; Friedrichs and Madsen, 1992; Gao and Collins, 1994; Dronkers, 1998; Wang et al., 1999; Whitehouse, 2006; Friedrichs, 2010; Townend, 2012; Dronkers, 2016; Zhou et al., 2017). These simple relationships prove to be useful not only for indicating morphological equilibrium state, but more importantly for providing clues on the response of tidal basins and estuaries to increasing human activities, or accelerating sea level rise (Friedrichs et al., 1990; Dissanayake et al., 2012; van der Wegen, 2013), as well as for assessing the resilience or adaptation time of these vulnerable systems after human intervention (Wang et al., 2002; Dastgheib et al., 2008).

Specifically, tidal asymmetry (hereafter indicated by “TA”), i.e. the inequality of flood and ebb durations, has been widely used to derive such stability relationships and adopted as an indicator for predicting the further evolution of tidal basin and estuary morphologies. TA is generated by the distortion of tidal waves propagating on continental shelves and entering basins or estuaries, and is termed as flood dominance if the flood duration is shorter (and flood velocity is larger) than the ebb, while the opposite condition is called ebb dominance. This has been extensively discussed in a wide literature in terms of field observations, theoretical analyses and numerical modelling because of its importance in producing the residual sediment transport which in turn essentially determines the long-term morphological evolution of tidal systems (see, e.g. Dronkers, 1986, 1998; Wang et al., 1999; Brown and Davies, 2010; Nidzieko and Ralston, 2012).

From a hydrodynamic point of view, the distortion of tidal wave during propagation can be represented as the non-linear growth of harmonics of the principal astronomical constituents, particularly the semi-diurnal constituent M_2 and its first harmonic overtide M_4 (Boon and Byrne, 1981; Aubrey and Speer, 1985). As an example, the distorted tidal sea-surface (η) and velocity (u) may be approximated by a superposition of M_2 and M_4 as (Friedrichs and Aubrey, 1988):

$$\eta = a_{M_2}\cos(\omega t - \theta_{M_2}) + a_{M_4}\cos(2\omega t - \theta_{M_4}) \tag{1a}$$

$$u = U_{M_2}\cos(\omega t - \phi_{M_2}) + U_{M_4}\cos(2\omega t - \phi_{M_4}) \tag{1b}$$

where t is time, ω is the M_2 tidal frequency (and hence the M_4 tidal frequency is 2ω), a is the tidal height amplitude, U is the tidal velocity amplitude, θ is the tidal height phase, and ϕ is the tidal velocity phase.

The relative sea-surface phase difference of M_4 and M_2 ($\theta = 2\theta_{M_2} - \theta_{M_4}$) generally indicates that a system is flood-dominant if $0 < \theta < \pi$ or ebb-dominant if $\pi < \theta < 2\pi$. Alternatively, the relative velocity phase difference of M_4 and M_2 ($\phi = 2\phi_{M_2} - \phi_{M_4}$) can also be used to indicate that a system is flood-dominant ($-\pi/2 < \phi < \pi/2$) or ebb-dominant ($\pi/2 < \phi < 3\pi/2$). The most significant flood-dominated and ebb-dominated conditions occur when the relative sea-surface phase differences (θ) are respectively $\pi/2$ and $3\pi/2$ (Figure 1a and c), or alternatively the relative velocity phase differences (ϕ) are respectively 0 and π (Figure 1b and d). The ratio of their amplitudes (a_{M_4}/a_{M_2} or U_{M_4}/U_{M_2}) suggests the significance of flood- or ebb-dominance. A number of studies have also highlighted the generation and characteristics of TA in areas that are subject to diurnal or mixed tidal regimes (Ranasinghe and Pattiaratchi, 2000; Nidzieko, 2010; Jewell et al., 2012).

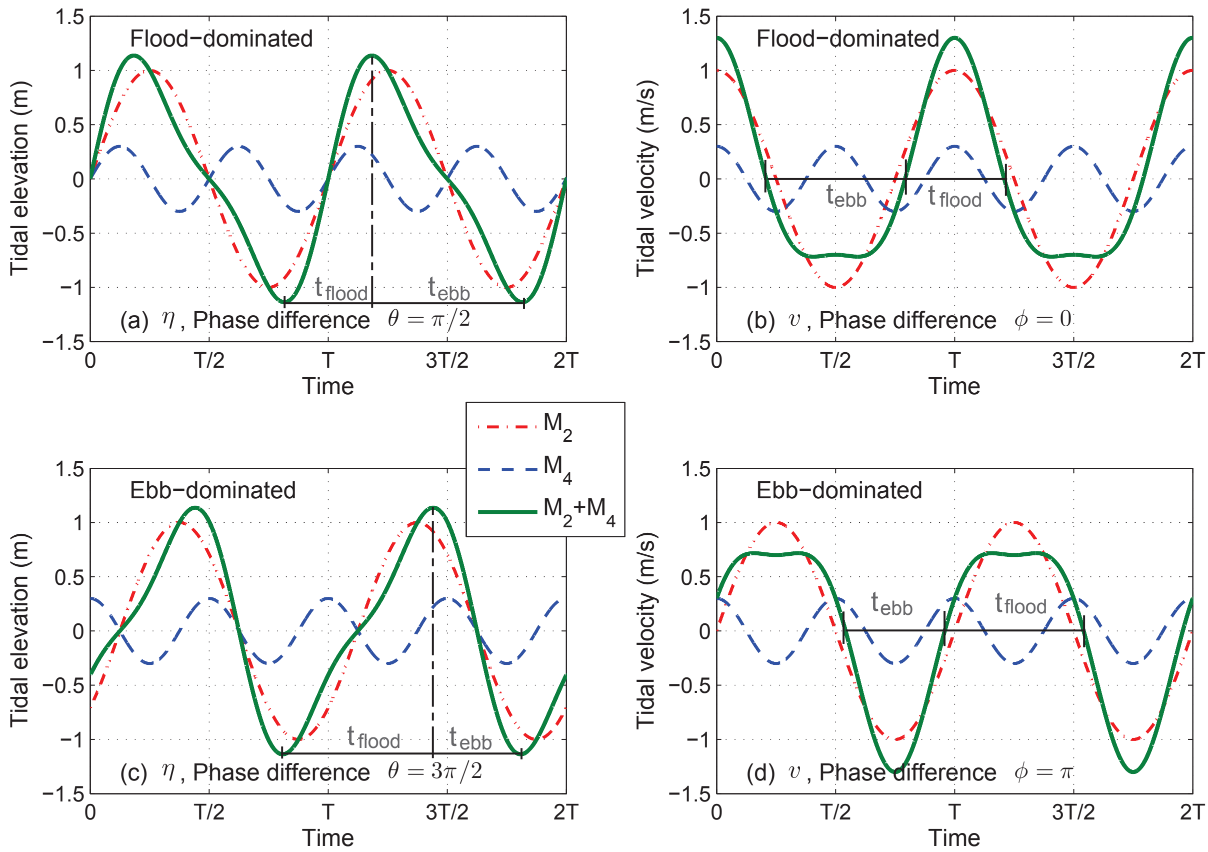

Figure 1: Examples of strongest tidal asymmetry conditions based on the superposition of the semi-diurnal constituent M_2 and its first harmonic overtide M_4. The M_2 tidal period T of the horizontal axis is approximately 12.42 hours. Panels (a) and (b) show strongest flood dominance using relative sea-surface and velocity differences (with shorter flood durations t_{flood}), while similarly panels (c) and (d) show strongest ebb dominance (with shorter ebb durations t_{ebb}). This figure is plotted following Friedrichs and Aubrey (1988).

The distorted tidal wave is one of the key contributors for residual sediment transport which generally occurs under two conditions (Dronkers, 1986): (1) unequal maximum flood and ebb velocities as the sediment transport responds non-linearly to velocities (mainly responsible for the transport of coarse sediment), and (2) unequal ebb and flood slack water periods during which sediments fall and settle (mainly influences the residual flux of fine sediment). Importantly, these two conditions can co-exist. Landward residual sediment transport is usually associated with flood dominance resulting in the infilling of tidal basins and estuaries, while seaward residual transport associated with ebb dominance leads to the erosion of the system. As long as the residual sediment transport exists, morphological changes will occur (Zhou et al., 2017). In other words, a morphologically stable state can only be present when residual sediment transport vanishes.

While TA has significant influence on the evolution of morphological features, the opposite is also true: the geometric characteristics of tidal basins and estuaries to a large extent determine the propagation of tidal waves, and hence promote the development of TA. In fact, tidal landforms tend to evolve to an equilibrium state by developing a morphology that offsets either flood dominance (resulting from, e.g. offshore TA or local baroclinic effects) or ebb dominance (resulting from, e.g. compensation for Stokes drift due to the phase lag between the times of high/low water and corresponding high/low slack water, or seaward fluvial discharge). Previous studies show that an estuarine system with large tidal flats tends to decrease flood tide duration and enhance the effects of channel friction, favouring flood dominance (Boon and Byrne, 1981; Aubrey and Speer, 1985; Dronkers, 1986). Conversely, a system of relatively deep channels with an absence of large intertidal flats generally promotes ebb dominance. Some studies have confirmed that TA and its associated residual sediment transport are gradually reduced when an evolving tidal system is approaching a morphologically stable state (e.g. Lanzoni and Seminara, 2002; van der Wegen and Roelvink, 2008; van Maanen et al., 2011; Guo et al., 2014). Recent studies based on numerical models also confirm that morphological equilibrium requires that the system adjusts itself towards reducing flood or ebb dominance (Dastgheib et al., 2008; Toffolon and Lanzoni, 2010; van der Wegen, 2013; Zhou et al., 2014b). Therefore, TA acts as an important indicator for the morphological state of a tidal system which may be in equilibrium (i.e. characterised by a vanishing TA) or potentially importing/exporting sediment (i.e. characterised by flood/ebb dominance).

In order to quantitatively describe the morphological state of tidal landforms, simple stability relationships between hydraulic parameters (e.g. tidal amplitude and water depth) and geometric form parameters (e.g. tidal channel/flat width, wet surface area and storage volume) have been developed based on either analytical or numerical studies. Though all the proposed stability relationships have been assessed in the context of real systems, few of them have been examined using an extensive worldwide dataset. Furthermore, none to our knowledge have been applied in conjunction with other methods to establish whether TA is a necessary and sufficient condition to determine equilibrium in these systems. Moreover, the applicability and the assumptions of these relationships have not been well examined. For instance, some relationships are derived based on a prismatic channel of constant width and depth, and hence their applicability to convergent systems remains questionable.

With the above in mind, the objectives of this study include: (i) to thoroughly review the existing theories and their associated stability relationships, clarifying their physical background; (ii) to inter-compare those relationships by conversions of the main geometric parameters (e.g. conversions between length, area and volume ratios); and (iii) to discuss their validity and applicability in comparison with the measured datasets that can be found in the literature. It must be stressed that this does not provide a validation of the relationships. It simply shows how real systems compare. A validation would require some independent measure of proximity to morphological stability and this is beyond the scope of this paper.

2 Theories and existing formulations

The one-dimensional (1D) tidal flow equations describing the conservation of mass and momentum are often used to explore the TA-based stability relationships, and read:

$$B\frac{\partial \eta}{\partial t} + \frac{\partial A_c u}{\partial x} = 0 \tag{2a}$$

$$\underbrace{\frac{\partial u}{\partial t}}_{\text{(i)}} + \underbrace{u\frac{\partial u}{\partial x}}_{\text{(ii)}} + \underbrace{g\frac{\partial \eta}{\partial x}}_{\text{(iii)}} + \underbrace{\frac{c_d u|u|}{h}}_{\text{(iv)}} - \underbrace{\frac{\partial}{\partial x}\left(\nu\frac{\partial u}{\partial x}\right)}_{\text{(v)}} = 0 \tag{2b}$$

where B is the cross-sectional width at water surface, h is the water depth at mean sea level, $A_c = B_c h$ is the flow-carrying cross-sectional area (B_c is averaged channel width), x is the longitudinal coordinate with $x = 0$ at estuary mouth, c_d is the bed friction coefficient and ν is the turbulence viscosity coefficient. To describe a funnelling tidal system which is commonly observed in nature, an exponentially converging function of channel width is often assumed ($B_c = B_{mo} \exp(-x/L_b)$, where B_{mo} is the channel width at estuary mouth and L_b is the convergence length, see e.g. Davies and Woodroffe, 2010). For a non-convergent channel, the value of convergence length tends to be infinity (i.e. $L_b = \infty$).

The underlined terms (i)-(v) in the momentum equation (2b) physically represent, one by one, the contributions of local inertia, advective inertia, slope gradient, bottom friction, and horizontal diffusion. Non-dimensional scaling analyses indicate that the advective inertia term (ii) and horizontal diffusion term (v) are small compared to other terms in shallow tidal basins and estuaries (Parker, 1991; Friedrichs, 2010; Dronkers, 2016) and hence can be neglected.

With terms (ii) and (v) eliminated, analytical solution of Equation (2) is possible when the friction term (iv) is linearised ($c_d u|u|/h = ru/h$, where $r = 8c_d U/3\pi$, U is the tidal velocity magnitude) and the cross-section is schematised (Figure 2). This analytical solution has been extensively explored using various techniques (e.g. Dronkers, 1998; Friedrichs, 2010; van Rijn, 2011; Toffolon and Savenije, 2011; Cai et al., 2012; Savenije, 2012; Winterwerp and Wang, 2013; Dronkers, 2016). The details are not repeated here while the theoretical background and the implications for this study are briefly introduced in the following sections.

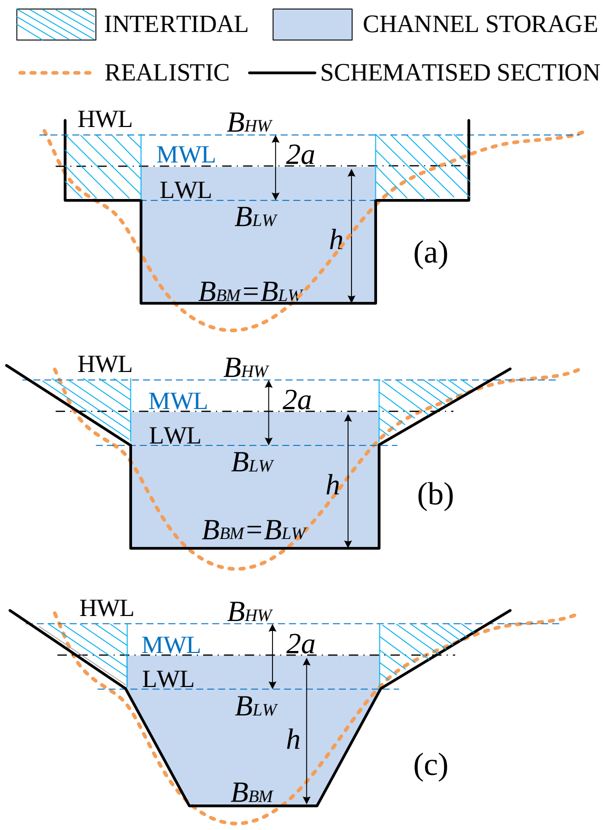

Figure 2: The schematic cross-sections adopted: (a) rectangular channel and flat used in Dronkers (1998), Winterwerp and Wang (2013), and Dronkers (2016), (b) rectangular channel and trapezoidal flat used in Friedrichs and Madsen (1992), (c) trapezoidal channel and flat used in Speer and Aubrey (1985), Friedrichs and Aubrey (1988), Friedrichs (2010) and Wang et al. (1999). B_{HW}, B_0 and B_{LW} are channel widths at high, mean and low water levels (HWL, MWL and LWL), B_{BM} is bottom channel width, a is tidal amplitude and h is mean channel depth.

2.1 Friedrichs-Aubery-Speer's approach

Based on the pioneering work of Aubrey and Speer (1985) and Speer and Aubrey (1985), Friedrichs and Aubrey (1988) concluded that two key parameters that can be used to determine the condition of TA are a/h (ratio between offshore tidal amplitude and mean water depth - taken to be the average channel depth in real systems) and V_S/V_C (ratio between the volume of intertidal storage and channel storage). They solved Equation (2) numerically (all terms included except the horizontal diffusion) and considered 84 combinations of channel geometries by varying channel depth and width (with other parameters set the same, i.e. channel length $= 7$ km, $c_d = 0.01$, $a = 0.75$ m, $B_{LW} = 2B_{BM} = 120(h - a)$, see Figure 2c).

Model results suggested that the morphologies of short and flood-dominated systems primarily change due to increased a/h whereas ebb-dominated systems primarily due to increased V_S/V_C. For small a/h (< 0.2), virtually all estuaries are ebb-dominant and for large a/h (> 0.3) all estuaries are flood-dominated while only when a/h is between 0.2 and 0.3, the system can be either moderately flood- or ebb- dominated, indicating equilibrium should be achieved at this range, depending on the other parameter V_S/V_C. Their findings are generally consistent with the measured data along the U.S. Atlantic Coast, and later studies have followed this theory to look at estuarine conditions (e.g. Wang et al., 2002; Dastgheib et al., 2008). The numerical model results are obtained under the following conditions: (1) non-convergent uniform trapezoidal cross-sections, and (2) short and shallow channels where friction dominates over inertia terms. Therefore, the numerically generated TA-based curve (see the red dashed line in Figure 3) should not be adopted as a universally valid indicator for all types of tidal basins and estuaries (e.g. convergent, long and deep tidal landforms).

Apart from the numerical curve introduced above, Friedrichs and Madsen (1992) and Friedrichs (2010) also developed several other stability relationships via analytical approaches. Based on perturbation analysis of the friction-dominated 1D tidal equations retaining only terms (iii) and (iv) of Equation (2b), Friedrichs and Madsen (1992) derived an explicit relationship using the schematic channel cross-section (Figure 2b), which reads:

$$\gamma_2 = \frac{5}{3}\frac{a}{h} - \frac{\Delta B}{B_0} \tag{3}$$

where B_{HW}, B_0 and B_{LW} are channel widths at high, mean and low water levels (m), respectively, $B_0 = 0.5(B_{HW} + B_{LW})$, $\Delta B = 0.5(B_{HW} - B_{LW})$ is the amplitude of change in channel width during one tidal cycle (m), and γ_2 is the non-dimensional TA parameter, flood and ebb dominance occur when $\gamma_2 > 0$ and $\gamma_2 < 0$, respectively. Hence, the morphological equilibrium state can be obtained theoretically when $\gamma_2 = 0$, and the following relation should be satisfied:

$$\frac{\Delta B}{B_0} = \frac{B_{HW} - B_{LW}}{B_{HW} + B_{LW}} = \frac{5}{3}\frac{a}{h} \tag{4}$$

More recently, Friedrichs (2010) performed a leading-term Taylor expansion for a linearised solution of tidal wave speed based on shallow non-convergent estuaries, giving an analytical relationship which slightly differs from Equation (3), and reads:

$$\gamma_6 = 2\frac{a}{h} - \frac{\Delta B}{B_0} \tag{5}$$

In order to directly compare this analytical solution with the former numerical curve in Friedrichs and Aubrey (1988), he converted $\Delta B/B_0$ to V_S/V_C based on the schematic cross-section in Figure 2b and another volume-type relationship was derived:

$$\frac{V_S}{V_C} = \frac{4\left(\frac{a}{h}\right)^2}{1 - 2\frac{a}{h}} \tag{6}$$

The comparison between Equation (6) and the numerical curve indicated that the analytical solution reasonably reproduces the fully non-linear results of Friedrichs and Aubrey (1988). The same analysis was also performed for shallow and funnel-shaped estuaries, indicating that the relations (Eqs. 5 and 6) also hold qualitatively.

2.2 Dronkers' theory

Based on the analytical solution of 1D tidal Equation (2b) retaining terms (i), (iii) and (iv), Dronkers (1998) also identified two key parameters S_{HW}/S_{LW} (ratio between the wet surface area at high and low water level) and H_{HW}/H_{LW} (or written as $(h+a)/(h-a)$, ratio between the average channel depth at high and low water level) to examine the TA conditions in the Dutch tidal basins. The schematic channel cross-section considered is shown in Figure 2a and the basin was assumed to be straight and longitudinally uniform. To facilitate a more in-depth understanding, the derivation is briefly introduced herein. Assuming that the solution to the simplified 1D tidal equation follows a harmonic function, the tidal elevation and velocity can be obtained:

$$\eta = \frac{1}{2} a_L \left\{ e^{-\mu(x-L)} \cos\left[k(L-x) - \omega t\right] + e^{\mu(x-L)} \cos\left[k(L-x) + \omega t\right] \right\} \tag{7a}$$

$$u = \frac{1}{2} \frac{a_L}{h} \frac{S}{S_c} \omega \left\{ e^{-\mu(x-L)} \cos\left[k(L-x) - \omega t - \varphi\right] - e^{\mu(x-L)} \cos\left[k(L-x) + \omega t + \varphi\right] \right\} \tag{7b}$$

with:

$$k = \sqrt{\frac{\omega^2}{2gh} \frac{S}{S_c} \left[1 + \sqrt{1 + \left(\frac{r}{\omega h}\right)^2}\right]} \tag{8a}$$

$$\mu = \sqrt{\frac{\omega^2}{2gh} \frac{S}{S_c} \left[-1 + \sqrt{1 + \left(\frac{r}{\omega h}\right)^2}\right]} \tag{8b}$$

$$a_L = \frac{a}{\sqrt{\cos^2(kL)\cosh^2(\mu L) + \sin^2(kL)\sinh^2(\mu L)}} \tag{8c}$$

$$\cos\varphi = \frac{k}{\sqrt{k^2 + \mu^2}} \tag{8d}$$

where ω is tidal frequency ($\omega = 2\pi/T$), a_L is tidal amplitude at landward boundary and L is the channel length (m), S and S_c are wet horizontal surface area and the wet horizontal channel surface area (m^2), respectively.

The times of high water (HW, t_{HW}) and low water (LW, t_{LW}) can be obtained by setting $\partial\eta/\partial t = 0$, and the times of high water slack (HWS, t_{HWS}) and low water slack (LWS, t_{LWS}) can be obtained by setting $u = 0$. For short tidal systems, Dronkers (1998) found that the following expressions can approximately hold at the estuary mouth ($x = 0$):

$$t_{HWS} - t_{HW} \approx \frac{L^2}{\omega} k_{HW} \mu_{HW} \tag{9a}$$

$$t_{LWS} - t_{LW} \approx \frac{L^2}{\omega} k_{LW} \mu_{LW} \tag{9b}$$

$$\text{with } k\mu = \frac{4}{3\pi} \frac{\omega c_d U}{g h^2} \frac{S}{S_c} \tag{9c}$$

Assuming a symmetrical tide at the estuary mouth (i.e. $t_{HW} - t_{LW} = \pi/\omega$), the flood duration can be obtained:

$$\Delta t_{flood} = \frac{\pi}{\omega} + \frac{L^2}{\omega}(k_{HW}\mu_{HW} - k_{LW}\mu_{LW}) = \frac{\pi}{\omega} + \frac{4L^2 c_d}{3\pi g}\left(\frac{U_{HW}}{h_{HW}^2}\frac{S_{HW}}{S_{c,HW}} - \frac{U_{LW}}{h_{LW}^2}\frac{S_{LW}}{S_{c,LW}}\right) \tag{10}$$

The duration of flood and ebb is equal (i.e. $= \pi/\omega$, or $T/2$) if $k_{HW}\mu_{HW} - k_{LW}\mu_{LW}$ is zero in Equation (10). To describe the asymmetrical condition, Dronkers (1998) defined a TA index:

$$\gamma_3 = \frac{k_{LW}\mu_{LW}}{k_{HW}\mu_{HW}} = \frac{S_{LW}}{S_{HW}}\left(\frac{h+a}{h-a}\right)^2 \frac{S_{c,HW}}{S_{c,LW}}\frac{U_{LW}}{U_{HW}} \tag{11}$$

where S_{HW} and S_{LW} are wet horizontal surface areas at high water and low water (m^2), respectively; $S_{c,HW}$ and $S_{c,LW}$ are the horizontal channel surface areas at high water and low water (m^2), respectively. A larger γ indicates a shorter flood duration and hence more flood-dominant characteristic.

For relatively deep channels, $S_{c,HW}$ and $S_{c,LW}$ can be assumed to be equal. However, for shallow basins with extensive flats, $S_{c,HW}/S_{c,LW}$ may be considerably larger than 1.0. Based on a number of Dutch tidal basins, the maximum velocities during HW and LW were assumed to have a similar magnitude ($U_{LW} \approx U_{HW}$), resulting in a simplified formulation of Dronkers' TA index:

$$\gamma_3 = \frac{S_{LW}}{S_{HW}}\left(\frac{h+a}{h-a}\right)^2 \tag{12}$$

In theory, a tidal system is in a stable configuration (when flood and ebb durations are approximately equal) if γ_3 equates to one. The field data of Dutch basins, however, show that γ_3 is often greater than 1.0 and $\gamma_3 = 1.21$ generally provides a good fit. The reasons that γ_3 is not exactly 1.0 can be many fold: (1) the terms $S_{c,HW}/S_{c,LW}$ and U_{LW}/U_{HW} in Equation (11) may not be assumed to be 1.0 for some tidal basins; (2) approximations of the quantities S_{HW}/S_{LW} and H_{HW}/H_{LW} measured in the field may not be accurate; (3) some assumptions for the derivation may not hold for certain tidal systems (e.g. many natural estuaries are not prismatic); and (4) the tide arriving at the estuary mouth can be asymmetrical.

In recognition of these limitations, Dronkers (2016) recently reconstructed the TA relationships using ratios of channel widths (typically at the mouth) instead of wet surface areas. One of the key assumptions is that a cyclic tide exists and can be used to represent the average sediment transport characteristics within the system over a long period. During this cyclic tide, the net sediment transport (which is assumed to vary as a function of flow velocity to the fourth power) is zero. Dronkers (2016) considered both non-convergent (i.e. channel width is constant) and convergent systems (i.e. channel width decreases exponentially from the mouth). The width-type stability relationships, for which the details of derivation can be found in Dronkers (2016), was obtained:

$$\frac{B_{HW} - B_{LW}}{B_{HW} + B_{LW}} = \gamma_9 \frac{a}{h} \tag{13a}$$

$$\text{for non-convergent basins: } \gamma_9 = \frac{7}{6} + \frac{h}{4a} \frac{\Delta t_{FR}^{mouth}}{\Delta t_S} \tag{13b}$$

$$\text{for convergent basins: } \gamma_9 = \frac{2p_1}{p_2 + 1/4} = f(L_b, r, k, \omega, h, h_s) \tag{13c}$$

where Δt_{FR}^{mouth} is the difference in duration of falling and rising tide at the mouth, Δt_S is the time delay given by the average between $t_{HWS} - t_{HW}$ and $t_{LWS} - t_{LW}$, and $\Delta t_S \approx rl^2/(3ghh_s)$, h_s is the representative water depth taking into account tidal flat, p_1 and p_2 are lumped parameters which can be expressed as functions of L_b, r, k, ω, h

and h_s (see Dronkers, 2016 for details).

Based on the analysis of field data, Dronkers (2016) found that the value of γ_9 generally falls in the range of 1.5 to 2.0 for the Dutch tidal basins. Depending on the local condition of the continental shelf of tidal basins, the offshore tidal wave can be already distorted and often with a shorter flood duration (i.e. $\Delta t_{FR}^{mouth} > 0$). Hence, the value of γ_9 is mostly larger than 7/6. Dronkers (2005) concluded that γ_9 is close to 2.0 for many tidal basins in Northwest European coast where the continental shelf is wide (tidal wave can be considerably distorted so Δt_{FR}^{mouth} is large), while γ_9 is close to 1.0 for tidal systems along the US Atlantic coast and UK east coast where the shelf is narrow. On the other hand, channel convergence can also affect the performance of TA-based relationships (e.g. via the convergence length L_b). Overall, the recent relationships (Equation 13) developed by Dronkers (2016) indicate that the value of TA index (γ_9) is highly site-dependent, and hence data points collected in tidal systems of different regions worldwide may show large scatter when a single relationship is used.

2.3 Wang's approach

Wang et al. (1999) built on the theories of Friedrichs and Aubrey (1988) and Dronkers (1998) and derived a relationship between a/h and V_S/V_C based on a similar cross-section geometry (assuming the channel bottom width $B_{BM} = 0.5B_{LW}$) as adopted by Friedrichs and Aubrey (1988). Wang's derivation also assumed: (1) frictionless tidal propagation ($c = \sqrt{gA/B}$, A and B are cross-sectional area and width) and (2) equivalent hydraulic water depth A/B at high and low water (implicitly assumes equivalent propagation speed at high and low water). The original derivation as presented in Wang et al. (1999) contains a minor error and was corrected in van der Wegen and Roelvink (2008) and has been applied as an indicator for equilibrium in a number of recent publications (e.g. van der Wegen et al., 2008; Dissanayake et al., 2012; van der Wegen, 2013). Under the assumptions of Wang et al. (1999), the following relation holds:

$$\frac{A_{HW}}{A_{LW}} = \frac{B_{HW}}{B_{LW}} \tag{14}$$

where A_{HW} and A_{LW} are the cross-sectional areas at high and low water (m^2), respectively. Following Wang et al. (1999), the same cross-section (Figure 2c, and assume $B_{BM} = 0.5B_{LW}$) is considered, hence the intertidal and channel storage volumes can be expressed as:

$$V_S = 2a(B_{HW} - B_{LW})L/2 \tag{15a}$$

$$V_C = (\frac{1}{2}B_{LW} + B_{LW})(h - a)L/2 + aB_{LW}L \tag{15b}$$

where L is the representative channel length. When the intertidal storage area is not considered as flow-carry part, the conveyance cross-sectional areas at LW and HW read:

$$A_{LW} = (\frac{1}{2}B_{LW} + B_{LW})(h - a)/2, \tag{16a}$$

$$A_{HW} = (\frac{1}{2}B_{LW} + B_{LW})(h - a)/2 + 2aB_{LW} \tag{16b}$$

However, if the intertidal storage area is considered as flow-carry part, the conveyance cross-sectional areas at LW and HW read:

$$A_{LW} = (\frac{1}{2}B_{LW} + B_{LW})(h - a)/2, \tag{17a}$$

$$A_{HW} = (\frac{1}{2}B_{LW} + B_{LW})(h - a)/2 + 2a(B_{LW} + B_{HW})/2 \tag{17b}$$

Combining Equations (14-15) with Equation (16), we obtain the original relationship by Wang et al. (1999) who did not consider the intertidal storage area as a flow-carrying part:

$$\frac{A_{HW}}{A_{LW}} = 1 + \frac{8}{3}\frac{\frac{a}{h}}{1-\frac{a}{h}} \tag{18a}$$

$$\frac{V_S}{V_C} = \frac{8}{3}\frac{\left(\frac{a}{h}\right)^2}{1-\frac{a}{h}}\left(\frac{3}{4}+\frac{1}{4}\frac{a}{h}\right)^{-1} \tag{18b}$$

If the intertidal storage area is considered as a part that can carry flow (flow-carrying), Equation (17) should be adopted instead of Equation (16), resulting in:

$$\frac{A_{HW}}{A_{LW}} = 1 + \frac{8}{3}\frac{\frac{a}{h}}{1-\frac{7}{3}\frac{a}{h}} \tag{19a}$$

$$\frac{V_S}{V_C} = \frac{8}{3}\frac{\left(\frac{a}{h}\right)^2}{1-\frac{7}{3}\frac{a}{h}}\left(\frac{3}{4}+\frac{1}{4}\frac{a}{h}\right)^{-1} \tag{19b}$$

The relationships represented by Equations (18) and (19) differ only because of the different definitions of the conveyance section. Based on Equations (18b) and (19b), a further consideration of the theory from Dronkers (1998) should result in the following equations:

$$\frac{V_S}{V_C} = \frac{8}{3}\frac{\left(\frac{a}{h}\right)^2}{1-\frac{a}{h}}\left(\frac{1+\frac{a}{h}}{1-\frac{a}{h}}\right)\left(\frac{3}{4}+\frac{1}{4}\frac{a}{h}\right)^{-1} \tag{20}$$

$$\frac{V_S}{V_C} = \frac{8}{3}\frac{\left(\frac{a}{h}\right)^2}{1-\frac{7}{3}\frac{a}{h}}\left(\frac{1+\frac{a}{h}}{1-\frac{a}{h}}\right)\left(\frac{3}{4}+\frac{1}{4}\frac{a}{h}\right)^{-1} \tag{21}$$

Compared with Equation (21), the minor difference in the derivation of Wang et al. (1999), i.e. Equation (20), is the factor 7/3 in the expression because of the exclusion of intertidal storage area as flow conveyance part. This will be further discussed in the following sections.

2.4 Overview of existing TA-based stability relationships

To the authors' knowledge, all the existing TA-based stability formulations describing the relationships between tidal morphologies and hydrodynamic parameters have been summarised in Table 1, which are referred to as R1-R9 for simplicity. All relationships were derived based on analytical methods except R1 which was numerically developed (Friedrichs and Aubrey, 1988). The formulation R8, linking S_{INT}/S_{HW} (the ratio between surface intertidal area and surface HW area) with a/h, was developed by van Maanen et al. (2013) for tidal network systems. Although this relationship was proposed through numerical experiments, we later find that it can be easily derived analytically by conversion from R3, and hence we categorise it as an analytical TA-based relationship. The original relationship R4 developed by Wang et al. (1999) does not include the intertidal storage area as flow-carrying, whereas R5 does.

Based on the considered geometric measure, these relationships can be generally categorised as width-type (R2, R6 and R9), area-type (R3 and R8) and volume-type (R1, R5 and R7). In the next sections, these three types of relationship are compared by writing the equations in terms of common geometric quantities (i.e. width, area and volume).

Table 1: List of existing TA-based stability relationships found in literature; refer to the text for the physical meaning of notations. Note: the relationship R5 (marked by '$*$') is derived based on Wang et al. (1999), but differently, the intertidal storage area is considered to be flow-carrying.

Index	Source	TA-based stability relationship	Cross-section
R1	Friedrichs and Aubrey (1988)	Numerical curve between $\frac{V_S}{V_C}$ and $\frac{a}{h}$	Figure 2c
R2	Friedrichs and Madsen (1992)	$\gamma_2 = \frac{5}{3}\frac{a}{h} - \frac{\Delta B}{B_0}$, where $\gamma_2 = 0$	Figure 2b
R3	Dronkers (1998)	$\gamma_3 = \left(\frac{H_{HW}}{H_{LW}}\right)^2 \frac{S_{LW}}{S_{HW}}$, γ_3 is site-dependent	Figure 2a
R4	Wang et al. (1999)	$\frac{V_S}{V_C} = \frac{8}{3}\frac{\left(\frac{a}{h}\right)^2}{1-\frac{a}{h}}\left(\frac{1+\frac{a}{h}}{1-\frac{a}{h}}\right)\left(\frac{3}{4}+\frac{1}{4}\frac{a}{h}\right)^{-1}$	Figure 2c
R5*	This study	$\frac{V_S}{V_C} = \frac{8}{3}\frac{\left(\frac{a}{h}\right)^2}{1-\frac{7}{3}\frac{a}{h}}\left(\frac{1+\frac{a}{h}}{1-\frac{a}{h}}\right)\left(\frac{3}{4}+\frac{1}{4}\frac{a}{h}\right)^{-1}$	Figure 2c
R6	Friedrichs (2010)	$\gamma_6 = 2\frac{a}{h} - \frac{\Delta B}{B_0}$, where $\gamma_6 = 0$	Figure 2b
R7	Friedrichs (2010)	$\frac{V_S}{V_C} = \frac{4\left(\frac{a}{h}\right)^2}{1-2\frac{a}{h}}$	Figure 2b
R8	van Maanen et al. (2013)	$\frac{S_{INT}}{S_{HW}} = \frac{a}{h}$	Figure 2a
R9	Dronkers (2016)	$\frac{B_{HW}-B_{LW}}{B_{HW}+B_{LW}} = \gamma_9\frac{a}{h}$, γ_9 is site-dependent	Figure 2a

3 Conversion and comparison

In the previous sections, we have reviewed the existing stability relationships that were derived based on TA analyses (Table 1). In order to gain more insight into these relationships, it is useful to compare their differences and similarities. However, this is not very straight-forward because different geometries were used to formulate these relationships. On the other hand, most of these relationships were only assessed against limited and specific measured datasets at a regional scale. For instance, the area-type relationship R3 developed by Dronkers (1998) was only examined for data of the Dutch tidal basins, and similarly the volume-type relationship R1 was only compared with the US data (Friedrichs and Aubrey, 1988). Therefore, it remains unclear how well these relationships work at the global scale and their applicabilities need to be better examined.

In this section, we present the conversions among different geometric ratios (i.e. V_S/V_C, S_{HW}/S_{LW}, S_{INT}/S_{SW}, and $\Delta B/B_0$) according to corresponding theoretically based schematic cross-sections (Figure 2). By doing this, different TA-based relationships can be compared directly.

3.1 Geometric conversion and datasets

The conversion should be conducted based on the cross-section adopted. For all cross-sections considered in Figure 2, the following relations on channel widths, wet surface areas and water depths hold to first order:

$$S_{HW} = B_{HW}L,\ S_{LW} = B_{LW}L \tag{22a}$$

$$S_{INT} = S_{HW} - S_{LW} \tag{22b}$$

$$H_{HW} = h + a,\ H_{LW} = h - a \tag{22c}$$

The major difference regarding the conversion among these three types of cross-sections is in the expressions for channel and storage volumes:

$$V_S = 2a(S_{HW} - S_{LW}),\ V_C = hS_{LW} \text{ (Figure 2a)} \tag{23a}$$

$$V_S = 2aL\Delta B,\ \Delta B = (B_{HW} - B_{LW})/2,\ V_C = hLB_{LW} \text{ (Figure 2b)} \tag{23b}$$

$$V_S = 2aL\Delta B,\ V_C = (B_{LW}/2 + B_{LW})(h - a)L/2 + aB_{LW}L \text{ (Figure 2c)} \tag{23c}$$

Using Equations (22) and (23), datasets of different geometric ratios can be interconverted, resulting in additional metrics for comparison (see Tables 2, 3 and 4 in the main text, and Table A1 in the appendix). Overall, four published datasets are considered in this study: (a) the Dutch area-type data (S_{HW}/S_{LW}) provided in Dronkers (1998), (b) the US volume-type data (V_S/V_C) in Friedrichs and Aubrey (1988), (c) the UK data in terms of both area and volume (S_{HW}/S_{LW} and V_S/V_C) in Townend (2005), and (d) the width-type data (B_{HW}/B_{LW}) collected in a few countries and provided in Dronkers (2016).

For the US data, as pointed out by Friedrichs and Aubrey (1988), the magnitude of the ratio a/h alone may indicate the overall TA condition in shallow estuaries of the US Atlantic coast. They found that only tidal basins with a/h falling in the range of 0.2-0.3 were close to equilibrium, hence only these locations in the US data are considered here for comparison. At the same time, it is worth noting that most of the relationships are derived based on the assumption that a/h is small. Therefore, from the UK dataset provided in Townend (2005), we only selected the tidal landforms with a value of a/h smaller than 0.5.

Table 2: Geometric parameters of the Dutch tidal basins. The left two ratios, S_{HW}/S_{LW} and H_{HW}/H_{LW}, are obtained from Dronkers (1998), and the rest are derived based on Equations (22) and (23a).

Data location	$\frac{S_{HW}}{S_{LW}}$	$\frac{H_{HW}}{H_{LW}}$	$\frac{a}{h}$	$\frac{V_S}{V_C}$	$\frac{S_{INT}}{S_{HW}}$	$\frac{B_{HW}-B_{LW}}{B_{HW}+B_{LW}}$
Western Scheldt	1.526	1.379	0.159	0.168	0.345	0.208
Eastern Scheldt	1.596	1.412	0.171	0.204	0.374	0.230
Texel Inlet	1.203	1.410	0.170	0.069	0.169	0.092
Eijerland Inlet	3.000	1.905	0.311	1.246	0.667	0.500
Vlie Inlet	1.688	1.644	0.244	0.335	0.407	0.256
Ameland Inlet	2.400	1.868	0.303	0.847	0.583	0.412
Pinkegat	4.462	3.000	0.500	3.462	0.776	0.634
Frysian Inlet	3.698	1.742	0.271	1.460	0.730	0.574
Lauwers Inlet	3.585	2.070	0.348	1.802	0.721	0.564
Ems-Dollard	1.810	1.56	0.219	0.355	0.448	0.288

Table 3: Geometric parameters of the US tidal basins for which the value of a/h is close to the range of 0.2-0.3. The left two ratios, a/h and V_S/V_C, are obtained from Friedrichs and Aubrey (1988), and the rest are derived based on Equations (22) and (23c).

Data location	$\frac{a}{h}$	$\frac{V_S}{V_C}$	$\frac{H_{HW}}{H_{LW}}$	$\frac{S_{HW}}{S_{LW}}$	$\frac{S_{INT}}{S_{HW}}$	$\frac{B_{HW}-B_{LW}}{B_{HW}+B_{LW}}$
Absecon, NJ	0.19	0.79	1.469	4.316	0.768	0.624
Strathmere, NJ	0.24	0.94	1.632	4.173	0.760	0.613
Townsend, NJ	0.25	1.14	1.667	4.653	0.785	0.646
Northam, VA	0.31	0.85	1.899	3.269	0.694	0.532
Little River, SC	0.25	0.73	1.667	3.373	0.703	0.543
North Inlet, SC	0.30	1.01	1.857	3.778	0.735	0.581
Price, SC	0.21	1.08	1.532	5.127	0.721	0.674
Capers, SC	0.22	0.68	1.564	3.488	0.611	0.554
Breach, SC	0.22	1.47	1.564	6.379	0.769	0.729
Folly, SC	0.21	0.88	1.532	4.363	0.676	0.627
Duplin, GA	0.21	0.91	1.532	4.478	0.684	0.635

Table 4: Geometric parameters of selected UK tidal basins and estuaries for which the value of a/h is smaller than 0.5. The left three ratios, a/h, V_S/V_C and S_{HW}/S_{LW}, are obtained from Townend (2005), and the rest are derived based on Equations (22) and (23c).

Data location	$\frac{a}{h}$	$\frac{V_S}{V_C}$	$\frac{S_{HW}}{S_{LW}}$	$\frac{H_{HW}}{H_{LW}}$	$\frac{S_{INT}}{S_{HW}}$	$\frac{B_{HW}-B_{LW}}{B_{HW}+B_{LW}}$
Teifi Estuary	0.223	0.038	1.703	1.573	0.413	0.260
Traeth Coch	0.229	0.170	2.470	1.593	0.595	0.424
Cromarty Firth	0.286	0.044	1.372	1.799	0.271	0.157
Firth of Tay	0.506	0.802	2.807	3.046	0.644	0.475
Firth of Forth	0.110	0.011	1.197	1.248	0.165	0.090
Tyninghame Bay	0.123	0.061	2.560	1.281	0.609	0.438
Blyth Estuary	0.197	0.875	6.295	1.491	0.841	0.726
Tyne Estuary	0.414	0.233	2.555	2.415	0.609	0.437
Tees Estuary	0.236	0.693	12.937	1.618	0.923	0.857
Ore-Alde-Butley	0.464	0.643	3.925	2.730	0.745	0.594
Thames Estuary	0.435	0.210	3.085	2.542	0.676	0.510
Medway Estuary	0.416	0.554	3.490	2.426	0.713	0.555
Portsmouth Harbour	0.494	0.179	2.155	2.951	0.536	0.366
Southampton Water	0.400	0.230	3.144	2.332	0.682	0.517
Newtown Estuary	0.374	0.209	1.963	2.197	0.491	0.325
Poole Harbour	0.396	0.207	1.613	2.314	0.380	0.235
The Fleet	0.453	0.569	3.802	2.655	0.722	0.584
Dart Estuary	0.387	0.173	1.776	2.261	0.437	0.279
Plymouth Sound	0.359	0.212	3.594	2.122	0.722	0.565
Falmouth	0.374	0.061	1.654	2.193	0.395	0.246
Helford Estuary	0.486	0.184	2.602	2.892	0.616	0.445

3.2 Volume-type relationships and comparison

The width-type relationships (R2 and R6 in Table 1) can be easily converted to volume-type using Equations (22) and (23). Based on the schematic cross-section (Figure 2b), Friedrichs (2010) converted R6 from width-type to volume-type relationship R7 to compare with a previous numerical result (Friedrichs and Aubrey, 1988). The relationship R2 can also be converted following Friedrichs (2010) using Equations (22) and (23b), resulting in another volume-type relationship:

$$\frac{V_S}{V_C} = \frac{\frac{10}{3}\left(\frac{a}{h}\right)^2}{1 - \frac{5}{3}\frac{a}{h}} \tag{24}$$

Similarly, the width-type relationship R9 derived by Dronkers (2016) can also be converted to volume-type equation following the same method. However, the cross-section as shown in Figure 2a should be used for consistency. Using Equations (22) and (23a) and we obtain:

$$\frac{V_S}{V_C} = \frac{4\gamma_9\left(\frac{a}{h}\right)^2}{1 - \gamma_9\left(\frac{a}{h}\right)} \tag{25}$$

where γ_9 is the TA index between 1.0 and 2.0, depending on local condition of tidal landforms.

The area-type relationship described by R3 (Table 1) can also be converted to volume-type by adopting the simplified cross-section (Figure 2a) as assumed by Dronkers (1998, 2016), reads:

$$\frac{V_S}{V_C} = 2\frac{a}{h}\left[\frac{1}{\gamma_3}\left(\frac{1+\frac{a}{h}}{1-\frac{a}{h}}\right)^2 - 1\right] \tag{26}$$

Assuming $\gamma_3 = 1$, i.e. theoretical equilibrium condition discussed before, Equation (26) can be simplified to:

$$\frac{V_S}{V_C} = \frac{8\left(\frac{a}{h}\right)^2}{\left(1-\frac{a}{h}\right)^2} \tag{27}$$

These volume-type relationships share some similarities in form and their comparison with datasets is shown in Figure 3. Except the numerical curve R1, all relationships are analytical and generally display a similar trend. With the increase of V_S/V_C, a tidal system becomes more ebb-dominated, while it becomes more flood-dominated in case of an increasing a/h. Most of the relationships are visually clustered within the range indicated by the two lines described by Equation (21) with different TA indices ($\gamma_9 = 1, 2$). According to (Dronkers, 2016), the value of γ_9 should be theoretically larger than 1.0 if the offshore tide is symmetrical. Therefore, it is reasonable to observe that other curves based on different approaches are all below the top dashed line (indicated by "Eq.21:γ_9=1").

The datasets from three different countries show considerable scatter. The UK data exhibit a large relative tidal amplitude (a/h) and a small relative intertidal storage (V_S/V_C), so it appears that most of the selected UK estuaries are flood-dominated. Although with a small relative tidal amplitude ($0.2 < a/h < 0.3$), the selected US tidal basins are largely ebb-dominated because of the relatively large intertidal storage. Differently, the Dutch data points mostly lie within the cluster of curves, indicating that many of these tidal systems could be considered to be close to equilibrium based on the theoretical arguments used. The converted curve with a TA index $\gamma_3 = 1.21$ appears to provide a better fit with the Dutch data than $\gamma_3 = 1$, which is consistent with Dronkers (1998). The value of relative tidal amplitude a/h for most of the Dutch basins in this dataset is close to the range of 0.2 to 0.3, which according to Friedrichs and Aubrey (1988) is close to equilibrium. Therefore, though developed via different approaches, the theoretical indications out of Dronkers (1998) and Friedrichs and Aubrey (1988) share some similar characteristics.

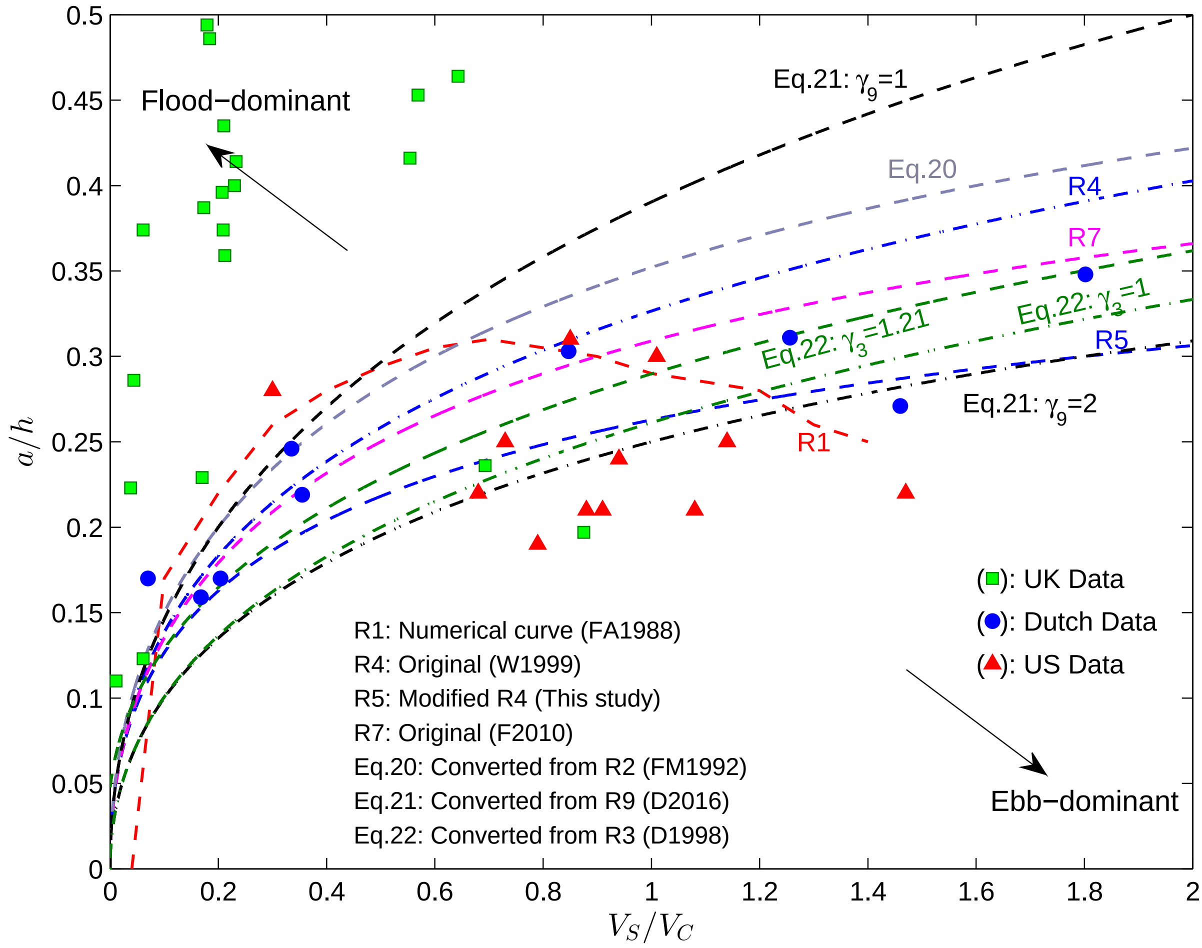

Figure 3: The existing and extended volume-type relationships between V_S/V_C and a/h as shown in Table 1 and derived in the main text. The points indicated by blue circles are the converted Dutch data from Dronkers (1998), red triangles are the original US data from Friedrichs and Aubrey (1988) and green squares are the original UK data from Townend (2005). Note the citations are shortened in the figure for simplicity (i.e. 'FA1988' = Friedrichs and Aubrey, 1988; 'F2010' = Friedrichs, 2010; 'W1999' = Wang et al., 1999; 'FM1992' = Friedrichs and Madsen, 1992; 'D1998' = Dronkers, 1998; 'D2016' = Dronkers, 2016) and this also holds for the following figures hereafter.

3.3 Area-type relationships and comparison

The volume-type relationship R5 can also be converted to area-type based on the trapezoidal cross-section (Figure 2c) following Wang et al. (1999). Using Equations (22) and (23c), we obtain:

$$\frac{S_{HW}}{S_{LW}} = 1 + \frac{8}{3}\frac{\left(\dfrac{a}{h}\right)}{1 - \dfrac{7}{3}\dfrac{a}{h}} = \frac{1 + 2\dfrac{H_{HW}}{H_{LW}}}{5 - 2\dfrac{H_{HW}}{H_{LW}}} \tag{28}$$

The width-type relationships R2, R6 and R9 in fact share the same mathematical form because the expressions $\Delta B/B_0$ and $(B_{HW} - B_{LW})/(B_{HW} + B_{LW})$ are equal. Taking R9 as an example, it can be easily transformed to area-type (using $S_{HW} = B_{HW}L$ and $S_{LW} = B_{LW}L$):

$$\frac{S_{HW}}{S_{LW}} = \frac{(1+\gamma_9)\dfrac{H_{HW}}{H_{LW}} + (1-\gamma_9)}{(1-\gamma_9)\dfrac{H_{HW}}{H_{LW}} + (1+\gamma_9)} \tag{29}$$

where γ_9 is equal to 5/3 and 2 for the conversion of R2 and R6, respectively.

The above-discussed area-type relationships in terms of S_{HW}/S_{LW} are compared in Figure 4. Except the curve indicated by "Eq.25:γ_9=1", all other relationships are relatively close in position and cluster within a narrow area. Comparable to the volume-type relationships, the horizontal axis S_{HW}/S_{LW} represents the capacity of intertidal storage and a larger S_{HW}/S_{LW} indicates a more ebb-dominated characteristic. The vertical axis H_{HW}/H_{LW} is somehow comparable to the relative tidal amplitude a/h and its increase indicates a more flood-dominated characteristic. They both reflect the potential for different propagation speeds at high and low water, which is the underlying cause of tidal asymmetry.

Similarly to Figure 3, the datasets of three different countries also show great scatter in the area-type plot (Figure 4), indicating the inherent consistency of these geometric ratios. The selected UK tidal landforms tend to be flood-dominated, while the US ones are mostly ebb-dominated. The Dutch tidal basins are generally close to equilibrium state, with points distributing around the curve R3 when $\gamma_3 = 1.21$. This is consistent with Dronkers (1998).

Many square points representing the UK estuaries appear to distribute around the converted equilibrium curve indicated by "Eq.25:γ_9=1" and away from the cluster of curves. The US estuaries tend to fall below the cluster of curves. Whilst this may say something about relative TA in these systems, the results are not providing a clear indication of relative stability.

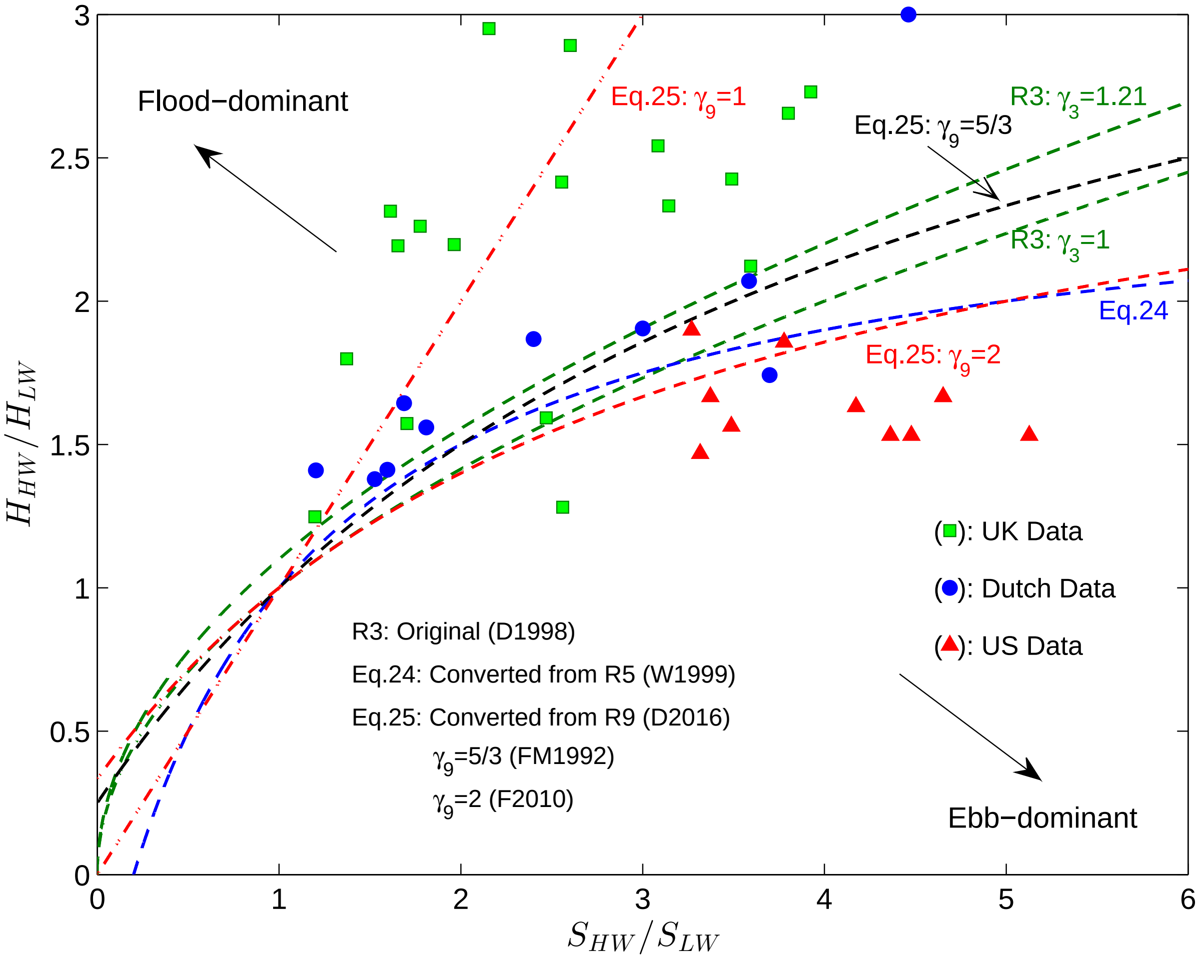

Figure 4: The existing and extended area-type relationships between S_{HW}/S_{LW} and H_{HW}/H_{LW} as shown in Table 1 and derived in the main text. The points indicated by blue circles are the original Dutch data from Dronkers (1998), red triangles are the converted US data from Friedrichs and Aubrey (1988) and green squares are the original UK data from Townend (2005).

Based on the theory of Dronkers (2005), van Maanen et al. (2013) further defined a “relative intertidal area” as the ratio between surface intertidal area (S_{INT}) and the total surface area inundated at high tide (S_{HW}), see R8 in Table 1. Though lacking a rigorous mathematical proof, the result of their numerical experiments for reproducing long-term evolution of tidal networks agreed quite well with the linear area-type relationship R8. Here we present a short derivation which may explain why the relationship R8 works for shallow tidal network systems. Recalling relationship R3 from Dronkers (1998) , we assume $S_{INT} = S_{HW} - S_{LW}$ as a first approximation and hence:

$$\frac{S_{INT}}{S_{HW}} = 1 - \frac{S_{LW}}{S_{HW}} = (1 - \gamma_3^2) + \frac{\gamma_3^2}{\left(\frac{1 + a/h}{2}\right)^2} \frac{a}{h} \tag{30}$$

For the models considered in van Maanen et al. (2013), γ_3 is 1.0 when the theoretical equilibrium condition is reached, hence the first term at the right hand side of the equation becomes zero and the second term can be simplified to a/h for shallow tidal network systems (a and h can be close where tidal flats are present). Therefore, Equation (30) can be simplified to relationship R8 which may be used as a first-order indicator for shallow tidal network systems.

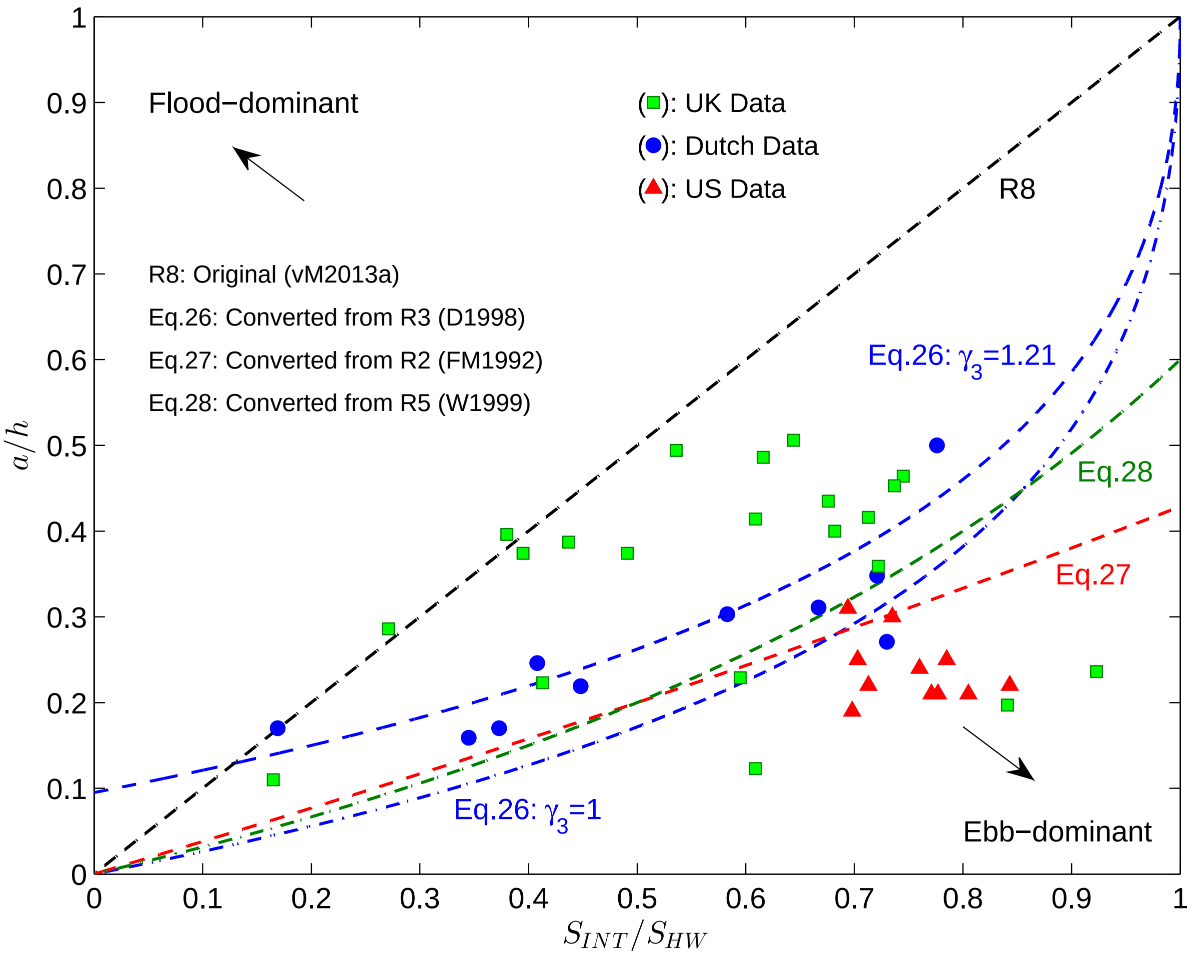

Figure 5: The existing and extended area-type relationships between S_{INT}/S_{HW} and a/h as shown in Table 1 and derived in the main text. The points indicated by blue circles are the original Dutch data from Dronkers (1998), red triangles are the converted US data from Friedrichs and Aubrey (1988) and green squares are the original UK data from Townend (2005). The shortened citation 'vM2013a' indicates van Maanen et al. (2013).

It is also interesting to rewrite the relationships developed by Friedrichs and Madsen (1992) and Wang et al. (1999) using S_{INT}/S_{HW} since this would provide a more direct indication for a tidal system with extensive tidal flats. We recall relationship R2 and use Equation (22), resulting in:

$$\frac{S_{INT}}{S_{HW}} = 2\left(1 - \frac{1}{1 + \frac{5}{3}\frac{a}{h}}\right) \tag{31}$$

Similarly, the relationship proposed by Wang et al. (1999) can also be easily converted to area-type (S_{INT}/S_{HW}) by using Equation (28):

$$\frac{S_{INT}}{S_{HW}} = 8\left(1 - \frac{1}{1 + \dfrac{1}{3}\dfrac{a}{h}}\right) \tag{32}$$

A comparison of these S_{INT}/S_{HW} area-type relationships is shown in Figure 5. Since S_{INT}/S_{HW} is converted directly from S_{LW}/S_{HW}, the overall performance of these relationships are comparable to Figure 4. The converted relationship from R3 in Dronkers (1998), indicated here by Eq.26, shows a better agreement with the Dutch dataset when γ_3 is 1.21. Similarly with previous figures, the UK data points lie mostly in the flood-dominated zone while the US data are mainly located in the ebb-dominated zone.

It is noted that the numerically inferred linear relationship R8 by van Maanen et al. (2013) is located far from the cluster of other TA-based curves. Visually, all tidal landforms from three different countries can be categorised as ebb-dominated using R8, which is inconsistent with other theories and previously published findings (e.g. Friedrichs and Aubrey, 1988; Dronkers, 1998; Townend, 2005). However, R8 appears to define an upper flood-dominant bound of these TA-based relationships. The amount of intertidal area increases as tidal range increases, which appears to hold even for systems that are almost all intertidal. For these systems, the tidal distortion between high and low water tends to be large and favors flood-dominance. Although R8 appears to work well with numerically produced tidal network systems, its applicability to natural tidal basins and estuaries merits further research.

3.4 Width-type relationships and comparison

Recently, Dronkers (2016) reformulated the TA-based relationships using widths instead of surface areas. The essence of the two types of TA-based stability relationships is the same, so Dronkers (2016) defined the ratio $(B_{HW} - B_{LW})/(B_{HW} + B_{LW})$ as relative intertidal area. In fact, one may convert the original area-type relationship R3 developed by Dronkers (1998) to width-type using Equation (22), and this reads:

$$\frac{B_{HW} - B_{LW}}{B_{HW} + B_{LW}} = \frac{\left(1 + \dfrac{a}{h}\right)^2 - \gamma_3 \left(1 - \dfrac{a}{h}\right)^2}{\left(1 + \dfrac{a}{h}\right)^2 + \gamma_3 \left(1 - \dfrac{a}{h}\right)^2} \tag{33}$$

when γ_3 is 1.0, as assumed in several studies, the above expression becomes:

$$\frac{B_{HW} - B_{LW}}{B_{HW} + B_{LW}} = \frac{2\dfrac{a}{h}}{1 + \left(\dfrac{a}{h}\right)^2} \approx 2\frac{a}{h} \tag{34}$$

One can immediately notice that the above simplified relationship (assuming a/h is small) converted from Dronkers' area-type relationship R3 shares a consistent form with the recently-developed R9. Noticeably, it also coincides with the width-type relationship R6 developed by Friedrichs (2010).

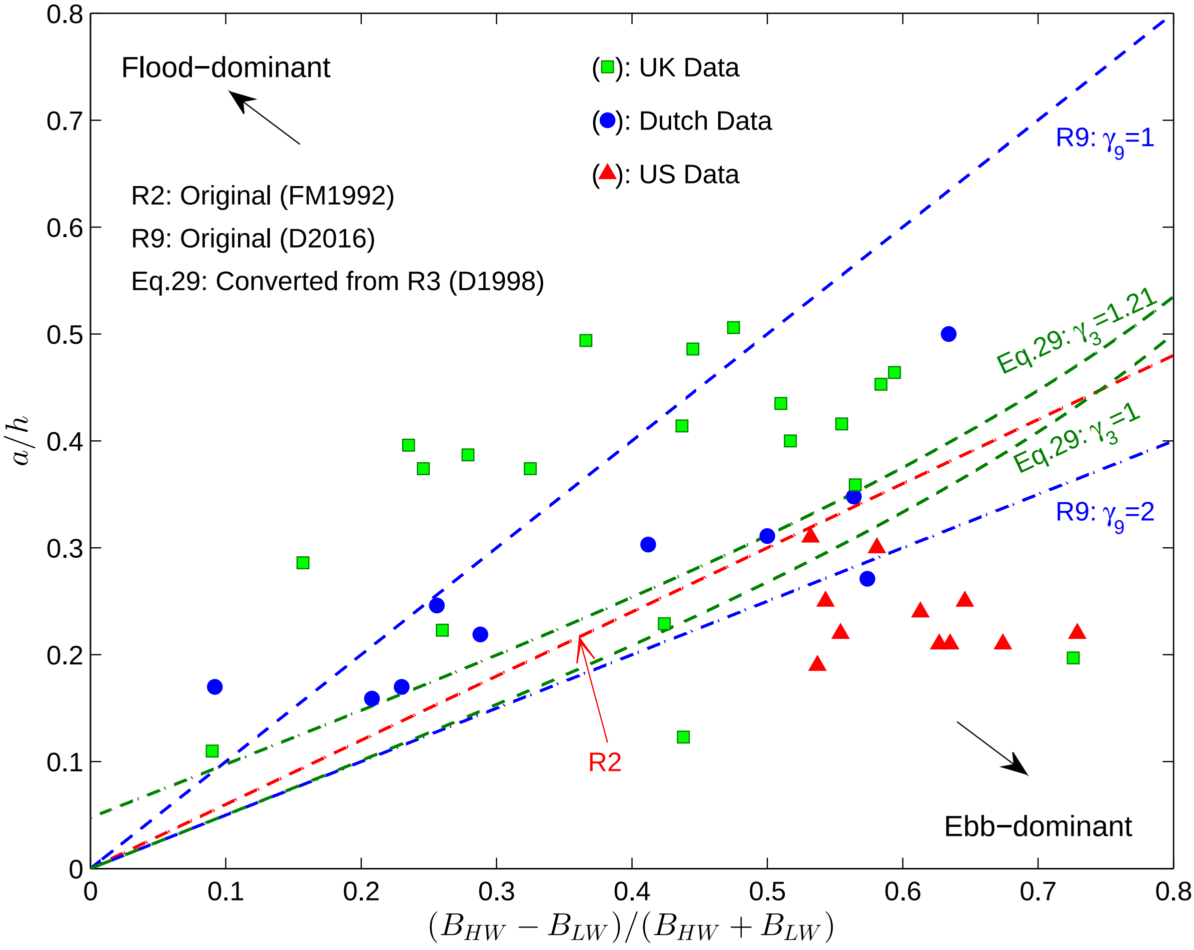

Figure 6: The existing and extended width-type relationships between $(B_{HW} - B_{LW})/(B_{HW} + B_{LW})$ and a/h as shown in Table 1 and derived in the main text. The points indicated by blue circles are the converted Dutch data from Dronkers (1998), red triangles are the converted US data from Friedrichs and Aubrey (1988) and green squares are the converted UK data from Townend (2005).

Dronkers (2016) compared the width-type relationship 'R9' with extensive datasets, ranging from short tidal lagoons to long convergent estuaries, which will be further discussed in the next section. Here we focus on the comparison of existing and converted TA-based relationships, as well as their comparison with the three published datasets (Figure 6). Not surprisingly, all of these relationships cluster within a certain narrow region as shown in previous figures, indicating the consistency among the geometric transformations. The overall spatial distribution of curves and data points in this width-type plot are particularly similar to the area-type (S_{HW}/S_{LW}) plot shown in Figure 4, indicating the inherent consistency between Dronkers (1998) and Dronkers (2016).

Similarly, the horizontal axis, $(B_{HW} - B_{LW})/(B_{HW} + B_{LW})$, physically represents intertidal storage whose increase leads to a more ebb-dominated system. Using the cluster of TA-based relationships (excluding the curve "R9:γ_9=1" as discussed before), it is evident that the UK data points tend to distribute within the flood-dominated zone while the US points in the ebb-dominated zone. The selected Dutch basins are mostly close to the purported equilibrium, as also discussed before. As demonstrated by Dronkers (2016), the TA condition for different tidal systems should be viewed as site dependent i.e. as a function of offshore difference in duration of falling and rising tide, channel convergence length and some other factors (see Equation 13). This will be further elaborated in the Discussion section.

4 Discussion

Simple estuarine stability relationships, either theoretical or (semi-)empirical, are particularly welcome by coastal scientists and engineers because they are normally easy to use and capable of providing a rapid assessment on the morphological condition of the tidal system. The most well-known of these is probably the (semi-)empirical relationship between tidal prism and cross-sectional area (hereafter shorted as "PA relation"). While the traditional PA relation has been under continuous exploration and widely adopted as an indicator of estuarine equilibrium (D'Alpaos et al., 2010; Zhou et al., 2014a), the theoretically inferred TA-based relationships have been paid much less attention.

We have reviewed the three types of TA-based relationship formulated using different geometries. Comparison of these relationships suggests an inherent consistency among them. The TA condition of tide-dominated landforms is chiefly governed by the competition between two physical parameters: the relative intertidal water storage and the relative tidal amplitude (Friedrichs and Aubrey, 1988; Wang et al., 1999; Dronkers, 2016). The former is reflected by the three types of geometric ratio (e.g. $\Delta B/B_0$,

S_{HW}/S_{LW}, V_S/V_C) which affect the efficiency of water exchange, and subsequently influence the duration of flood and ebb tide. The latter, reflected by a/h, plays a major role in determining the contribution of bottom friction on tidal flow propagation. A larger relative intertidal storage usually tends to slow down the flood tide, resulting in more ebb-dominated characteristic; while a larger relative tidal amplitude tends to considerably reduce the ebb velocity, favouring flood dominance.

Despite their simple form, the use of these TA-based relationships does not appear to be simple, primarily because of (i) what can be measured in practice; (ii) the implications of the assumptions made in the derivations; and (iii) uncertainties in the data and limitations in the current approaches to TA analysis. These issues may hinder the TA-based relationships being appropriately used in practice. In this section, we discuss these issues in detail and propose several future research directions.

4.1 Geometries assumed in 1D models and measured in practice

Based on the 1D tidal equations, the existing TA-based relationships are mostly derived by assuming a prismatic estuary with simple regular cross-sections (Figure 2). However, natural estuaries normally converge landwards both in width and depth, and are characterised by various irregular cross-sections (Figure 7). To make use of a 1D solution, the section that defines the conveyance (i.e. the flow-conveying section) is the key to getting representative hydrodynamics. This leads to a focus on propagation speed and hence the hydraulic radius or, for wide systems, hydraulic depth. Below, we will first introduce the approaches of estimating the conveyance section and the hydraulic depth from natural estuaries and then discuss their effects on TA-based relationships.

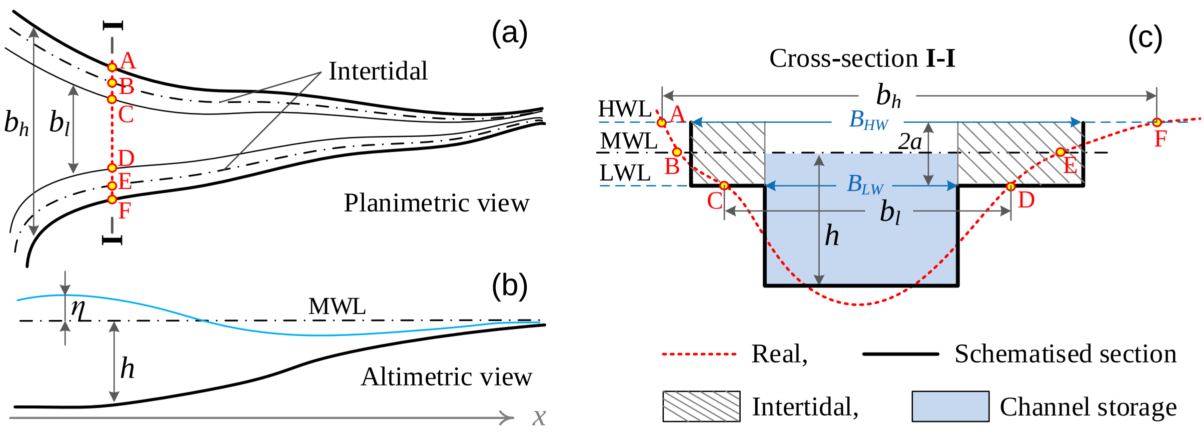

Figure 7: Sketch and geometrical parameters of an estuary. This figure is modified from Savenije (2012). Note that the measured widths at HWL and LWL (b_h and b_l) may be different from the ones of the schematised cross-section (B_{HW} and B_{LW}).

In practice, the geometric values of estuary width, surface area and volume are normally obtained at HWL and LWL (e.g. b_h and b_l in Figure 7a). These geometries can readily be extracted from charts, bathymetric surveys or satellite data. In addition, the tidal range at the estuary mouth can be measured and is usually known to a reasonable degree of accuracy. The mean values of parameters used in the 1D tidal equations (e.g. the mean hydraulic depth h, the mean estuary channel width B_{LW} and the mean estuary top width B_{HW}) can be estimated using these measured quantities. For example, Dronkers (1998) proposed the following relationships:

$$h = a + \frac{V_{LW}}{S_{LW}} \tag{35a}$$

$$B_{HW} = \frac{S_{HW}}{L} \tag{35b}$$

$$B_{LW} = \frac{S_{LW}}{L} \tag{35c}$$

where, V_{LW} is the volume at LWL, and L is the length of the estuary. However, some studies also suggested different formulations for the mean hydraulic depth. Using the Stour and Orwell estuaries as study cases, Roberts et al. (1998) found the following relation of the mean hydraulic depth could be more reliable:

$$h' = \frac{1}{2}(h_{HW} + h_{LW}) = \frac{1}{2}(\frac{V_{HW}}{S_{HW}} + \frac{V_{LW}}{S_{LW}}) \tag{36}$$

where, h_{HW} and h_{LW} are the mean water depth at HWL and LWL, respectively, V_{HW} is the volume at HWL. Townend (2005) also defined the hydraulic depth using volume and surface area at the mean tidal level:

$$h'' = \frac{V_{MW}}{S_{MW}} \tag{37}$$

where, V_{MW} and S_{MW} are respectively the volume and the surface area at MWL.

Based on the measured data of the UK estuaries, the performance of the three different expressions of the mean hydraulic depth (h, h', and h'') is compared against the volume-type TA relationships (Figure 8). Compared to the original Dronkers' expression (h, Equation 35a), the other two approaches tend to result in assessments of tidal asymmetry that are even more flood-dominant. Noticeably, just a different way of estimating the mean hydraulic depth dramatically changes the a/h values, resulting in markedly different distribution of data points in Figure 8. This points to an inherent sensitivity in the method, making quantitative application difficult to interpret in any meaningful way.

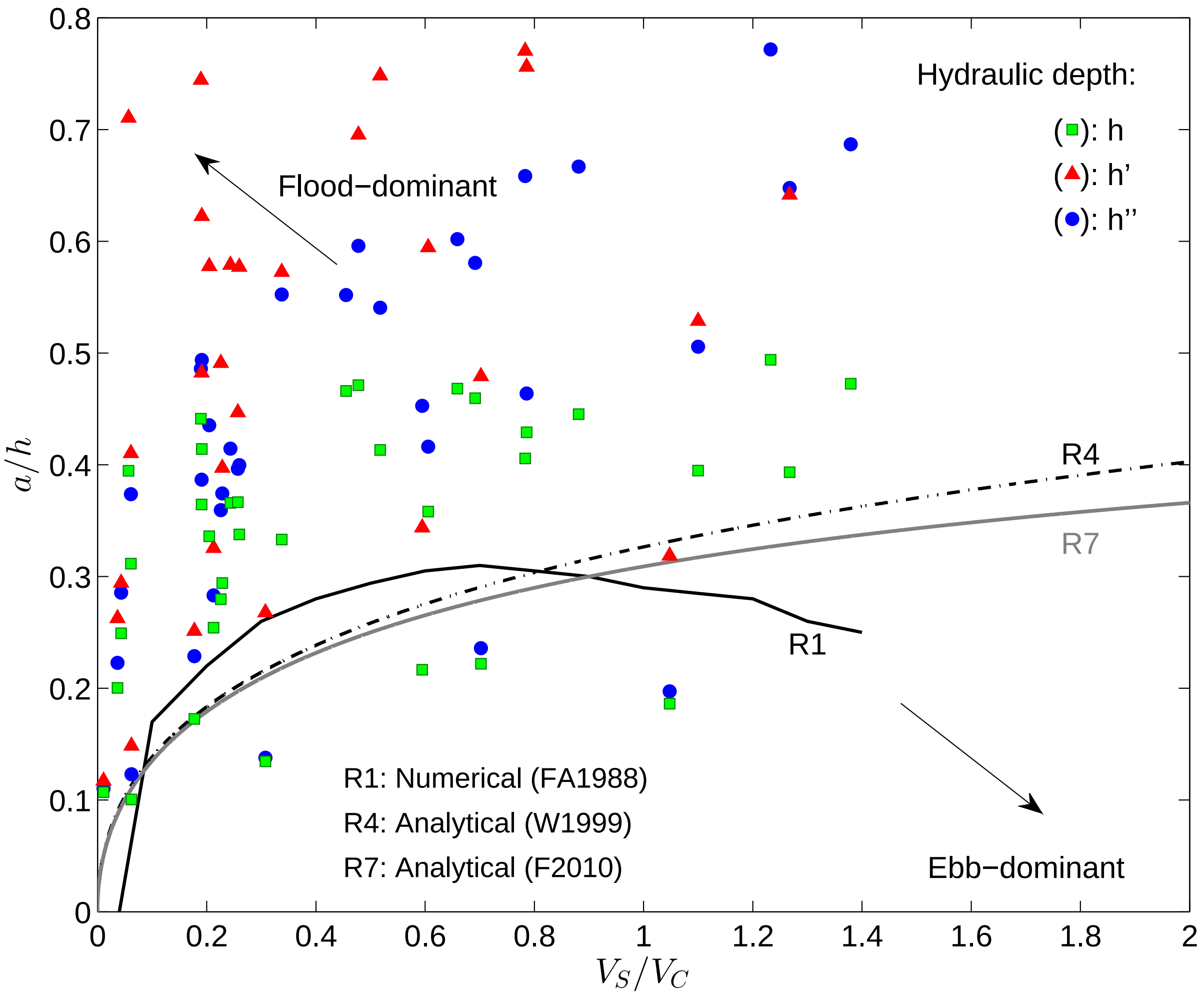

Figure 8: Different distributions of data points of a/h and V_S/V_C for different expressions of the mean hydraulic depth (h, h', and h''), based on the UK estuary data of Townend (2005).

To facilitate the 1D model solution, a highly related quantity is the so-called conveyance section. It is assumed, in most of the previous studies, that only the channel section (i.e. excluding intertidal area) is considered to be the flow-conveying part (Figure 7c). The influence of this assumption can be seen in Figure 3 by comparing the curves R4 and R5 obtained respectively excluding and including intertidal area as the flow-conveying part. Compared to R4, the stability curve obtained with intertidal area included (R5) tends to shift to the ebb-dominant side. This essentially means that an estuary has more possibility to be categorised as a flood-dominant system using R5 (because intertidal area effectively enhances bottom friction, and tends to result in flood-dominant tidal flow). The rationality of excluding or including the intertidal area as flow-conveying part, as well as its influence on the TA-based relationships, may be readily examined using a 2D tidal model. In reality, the presence of a shallow sub-tidal shoals can be found in many estuarine systems and this may also alter the effective conveyance section.

Our analysis, therefore, suggests that these relationships may be of limited value when used in isolation for management and conservation purposes. The key to appropriately applying the TA-based relationships is to ground the analysis in a way that ensures the celerity is correctly represented. Without some means of verifying the tidal wave propagation, these TA-based relationships should be used with extreme caution or not used to evaluate the condition of systems relative to equilibrium. In order to ensure the correctness and representativeness of these estimated mean geometries that are used in 1D models (and hence in TA-based relationships), it is vital to validate the analytical (or simulated) tidal hydrodynamics against field measurements or more sophisticated 2D numerical models. For example, contemporaneous data of water levels, velocities, tidal phases at two or more locations along the estuary can be used to estimate the celerity and hence confirm the geometric quantities such as the effective conveyance section, the intertidal storage and the hydraulic depth (e.g. Friedrichs and Aubrey, 1994; Cai et al., 2012; Savenije, 2012).

4.2 Applicability of TA-based relationships

Although these TA-based relationships display an overall consistency, it is still worthwhile to understand their physical background and hence applicability before choosing a specific one, particularly because different assumptions were made for their derivation. For example, different schematic cross-sections were assumed and different simplifications were made in the 1D tidal flow equations for analytical solutions. In fact, the recent theory of Dronkers (2016) indicates that the TA-based relationship appears to be site-dependent, because the TA index (γ_9) is a function of various site-specific parameters (Equation 13). In particular, the offshore difference in duration of the flood and ebb

(Δt_{FR}^{mouth}) is one of the major factors affecting the behaviour of TA-based relationships.

Dronkers (2016) compared the width-type relationship R9 with data collected from 39 tidal landforms worldwide, including 18 tidal lagoons and 21 convergent estuaries (Table A1). The comparison is shown in Figure 9. Noticeably, a large number of tidal lagoons and estuaries tend to distribute around the curve indicated by "R9:γ_9=2". According to Dronkers (2016), many of these tidal systems are close to equilibrium state. Overall, the distribution of data points roughly indicates that tidal landforms with a larger relative intertidal storage also have a larger relative tidal amplitude. In other words, the linear width-type relationship R9 is generally in agreement with field data.

However, a number of estuaries are also found to locate far from the curves, clustering within a narrow area defined by the value of $(B_{HW} - B_{LW})/(B_{HW} + B_{LW})$ being smaller than 0.1. Dronkers (2016) did not include the data points of these systems (i.e. indicated by grey markers in Figure 9) in his original plot because some of these estuaries have a large fluvial discharge compared to tidal discharge, and hence the TA-based relationships which assume a minor river influence do not hold anymore. Those estuaries that distribute close to the curve "R9:γ_9=2" are found to have a small river discharge compared to tidal discharge (e.g. WS, TH, DE, RI, DY and GO). Most of these estuaries have a positive offshore tidal asymmetry with a shorter flood duration ($\Delta t_{FR}^{mouth} > 0$), so their stability curves tend to move downward according to Equation 13, and hence the flood-dominant zone becomes larger in Figure 9. An exception is the Humber estuary (HB) for which Dronkers found Δt_{FR}^{mouth} to be zero, hence its TA-based stability relationship should have a relatively small γ_9 (i.e. the relationship should move upward). The same holds for the French tidal lagoon Bassin Arcachon (BA) which even has a negative Δt_{FR}^{mouth}. Typically, tidal systems with a wide continental shelf tend to have a large and positive Δt_{FR}^{mouth} due to the distortion of tidal wave during propagation, such as the Dutch basins. On the other hand, the interaction of the astronomical tides may result in a negative Δt_{FR}^{mouth} in some tidal systems such as the US Willapa Bay (WB). The reader is referred to Dronkers (2016) for more details.

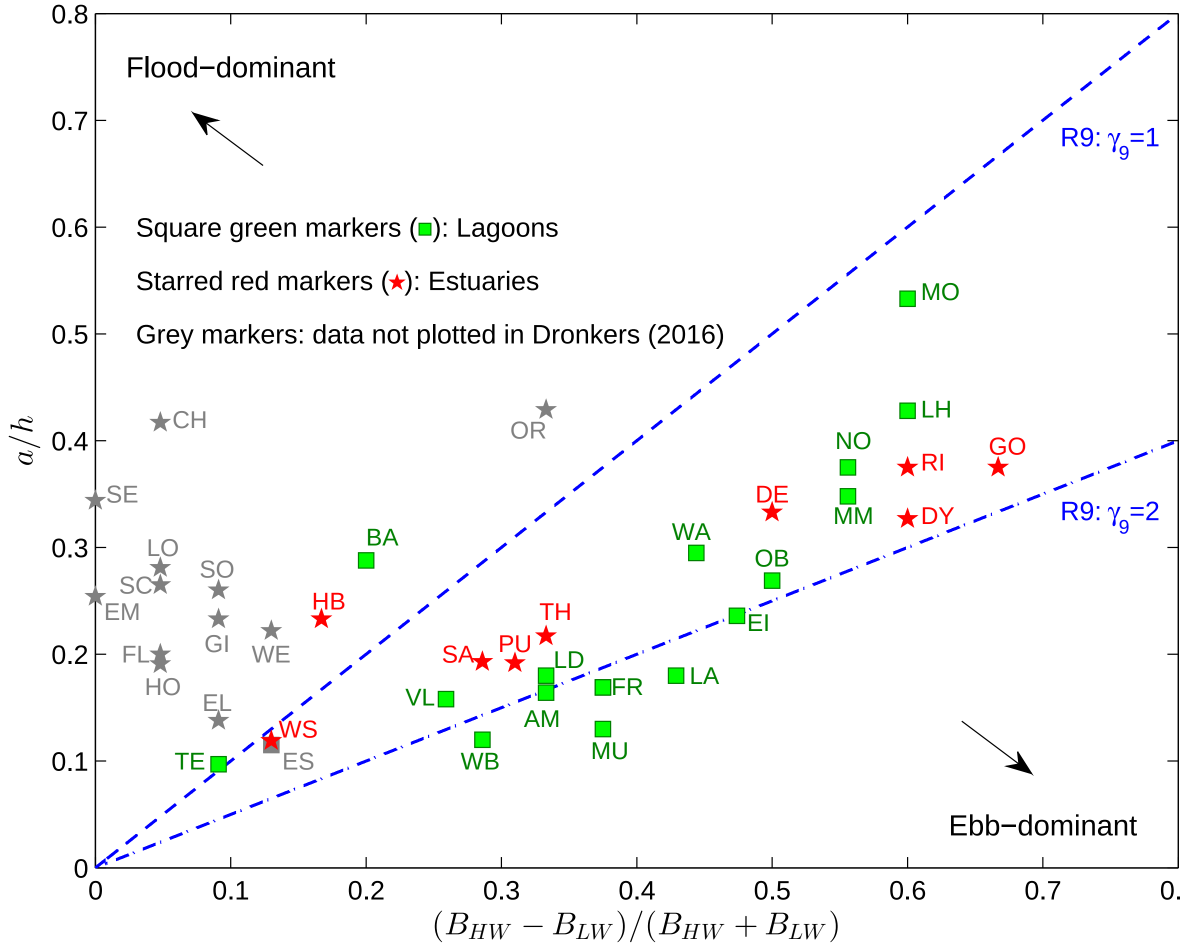

Figure 9: Comparison between datasets and width-type relationship R9 developed by Dronkers (2016). The data points indicated by stars indicate convergent estuaries, squares indicate short tidal lagoons. The grey markers indicate the data points that are not plotted in the original figure of Dronkers (2016), but shown in Table A1. The capital letters near the markers indicate specific tidal landforms of interest and discussed in the main text, refer to Table A1 for details. This figure is redrawn from Dronkers (2016).

Another point worth discussing is the influence of the planimetric estuary convergence which has been mostly neglected in existing studies. It is found that estuary convergence does not seem to play a significant role on the TA-based relationships, as also indicated by Friedrichs (2010). The 1D analytical solution of an exponentially convergent estuary proposed by Winterwerp and Wang (2013) can provide some insight. Following the work of Dronkers (2005) and Friedrichs (2010), they found that the TA index for convergent systems (γ_c) can be described by:

$$\gamma_c = \left[\frac{1+a/h}{1-a/h} \cdot \frac{\sqrt{(L_*^2 - (1-a/h))^2 + \left(\dfrac{L_*^2 r_*}{1-a/h}\right)^2} + (L_*^2 - (1-a/h))}{\sqrt{(B_* L_*^2 - (1+a/h))^2 + \left(\dfrac{B_* L_*^2 r_*}{1+a/h}\right)^2} + (B_* L_*^2 - (1+a/h))} \right]^{1/2} \tag{38}$$

where $L_* = 2\omega L_b/\sqrt{gh}$ is the dimensionless convergence coefficient, $r_* = r/\omega h$ is the dimensionless friction coefficient, and $B_* = B_{HW}/B_{LW}$. For friction-dominated systems (e.g. shallow tidal basins), Equation 38 can be simplified to:

$$\gamma_c \approx \frac{1+a/h}{1-a/h}\sqrt{\frac{1}{B_*}} = \frac{h+a}{h-a}\sqrt{\frac{B_{LW}}{B_{HW}}} \tag{39}$$

The above simplified equation does not include the convergence term anymore, so the effect of channel convergence on the performance of TA-based relationships is minor for shallow friction-dominated systems. One may notice that this simplified equation is consistent with Dronkers' theory and it shares a similar form as Equation (12) by assuming $B_{HW}/B_{LW} = S_{HW}/S_{LW}$. In fact, the derivation of these existing TA-based relationships has mostly considered the friction term as a major contributor in the momentum balance. Overall, it can be concluded that these TA-based relationships derived using prismatic channels should be equally applicable for shallow convergent systems such as tidal networks. However, owing to the spatially varying width of channels (often in an allometric relationship with depth), the width-type TA relationships may not be the best choice for convergent systems. As an alternative, the area- and volume-type relationships can be considered. While for non-convergent systems, the width-type stability relationships are most convenient to apply since it is relatively easy to collect the width data.

4.3 Uncertainties, limitations and further research

There are also a few uncertainties that need to be noted when applying these TA-based relationships. To start with, the accuracy of the measured data for comparison or validation needs careful examination. Because of the limitations and uncertainties in the measuring approaches and techniques, the data collected in large-scale estuarine systems are usually not very accurate. For example, Townend (2005) found that the percentage differences between two studies in estimates of bulk properties of nine UK estuaries range from approximately 30% to 150%. The accuracy of data may bring uncertainties and difficulties in the interpretation of results when stability relationships are used. For example, the generality and applicability of the empirical PA relation which was originally fitted from the US observational data has been much debated (Gao and Collins, 1994; Townend, 2005; Zhou et al., 2014b). It is also noted that there are some inconsistencies in the Dutch data between Dronkers (1998) and Dronkers (2016). Apart from the reason that the data were measured in different years, it may also originate from different measuring approaches and techniques. In order to apply these stability relationships with more confidence, it is necessary to develop advanced data collecting and processing methodologies to ensure sound comparisons and validations. It may be worth noting that the more detailed swath and LiDAR datasets that are now becoming available may enable improved estimates of gross properties to be derived in the future. Another uncertainty is on the dominant processes that shape the morphology of tidal basins and estuaries. Different processes besides tidal currents may also play an important role in some tidal basins and estuaries. For example, using a combination of hydrodynamic measurements and sediment deposition records, Hunt et al. (2016) demonstrated that waves can be morphologically significant by influencing tidal and suspended sediment flux asymmetry (see also e.g. Green and Coco, 2014). Another commonly overlooked factor when formulating the TA-based relationships is the baroclinic effect that can alter the 3D flow structure, sediment settling and subsequently affect the morphological evolution of estuaries and tidal basins (Geyer and MacCready, 2014; Gong et al., 2014). Therefore, the relative contribution of these factors to shaping estuarine morphology compared to barotropic tides should be evaluated before the TA-based relationships can be used.

A final comment is made on the limitations of these TA-based relationships. First, a number of assumptions were made to derive these relationships, including e.g. schematic cross-sections and simplified 1D tidal equations. Hence, these relationships should not be considered universally valid and their physical indications on natural systems should be interpreted in a qualitative sense rather than a quantitative sense. For instance, the theory of Dronkers (1998) is mostly applicable for relatively short tidal basins with a symmetrical offshore tidal boundary and the approach of Friedrichs and Aubrey (1988) and Friedrichs1992 is for shallow friction-dominated systems. Second, the derivation of these relationships is mainly based on the ratio between flood and ebb durations (or the ratio between peak flood and ebb velocities) from purely a hydrodynamic perspective. However, the morphological indications are sometimes not so straight-forward. This is an issue that is deeply embedded in the literature and reflects the dominance of hydraulic approaches over morphological ones. For example, some UK estuaries are found to export coarse sediment due to the ebb-dominated asymmetry in peak velocities and import fine sediment due to flood-dominated asymmetry in slack water durations. Third, TA is not the only factor determining the residual sediment transport (and hence morphological change) while other factors such as river discharge and compensation flow for Stokes drift can also play a role (Guo et al., 2014). Therefore, the TA-based relationships should be applied with care, taking into account the many influencing factors. Further research should be considered to (1) compare these TA-based relationships with more accurate field datasets and 2D numerical models, (2) relax some of the assumptions to develop more generic formulations, and (3) explore the morphodynamic basis of equilibrium to develop an approach that more appropriately defines system stability.

5 Conclusions

A synthesis of theories and formulations describing the relation between estuarine morphology and tidal asymmetry (TA) is provided in this study. Three different types of TA-based relationships, formulated using ratios of storage volumes, surface areas and basin widths, are discussed. These three geometric ratios are inter-converted to formulate additional stability relationships of the same metrics, so that different theories and approaches can be compared. The comparison indicates that most of these TA-based relationships tend to cluster within a narrow range, indicating the agreement among different theories. The relative intertidal storage reflected by the three types of geometric ratios (e.g. $\Delta B/B_0$, S_{HW}/S_{LW}, V_S/V_C), and the relative tidal amplitude reflected by a/h, are the two major controlling factors to determine the TA condition of a tide-dominated system.

Four published datasets are considered to compare with these different types of TA-based stability relationships. Against these data, a generally consistent indication of the TA condition is shown using different relationships, implying their inherent consistency. Depending on the data available, different relationships can be considered for practical use (e.g. estimation of a tidal system in response to short-term human interventions and long-term climate change). However, all the TA-based relationships are developed inevitably under various assumptions and their physical significance for natural systems should be interpreted with care. This is particularly the case when analysing a variety of tidal landforms with different types of hydrodynamic, sedimentologic and landscape settings.

The scatter exhibited by the various relationships is notably less significant than the scatter exhibited by the measured data. Given the expectation that most systems are responding to changes such as sea level rise and the nodal tide, suggests they are tracking some form of equilibrium, albeit with a lag (Wang and Townend, 2012). This leads to the conclusion that whilst these relationships provide some information about the tidal conditions, whether this provides a robust basis for determining morphological stability remains an open question. Therefore, the use of these methods for management and conservation points to a clear need. Whether they are fit for purpose is, however, clearly questionable. There is therefore a need for research that explores the morphological basis of equilibrium, to develop and, importantly, validate an approach that more clearly identifies appropriate measures of system stability.

Acknowledgements

This study is supported by the Natural Science Foundation of Jiangsu Province (Grant No. BK20160862), the National Natural Science Foundation of China (NSFC, Grant Nos. 41606104, 51620105005), the National Key Research and Development Program of China (Grant No. 2016YFC0401505) and the Fundamental Research Funds for the Central Universities (Grant No. 2016B00714). We highly appreciate two anonymous reviewers and the editors for their constructive comments. This is a ZORC contribution 1701.

757 # Appendix

Table A1: Geometric parameters of short tidal lagoons and convergent estuaries adapted from Dronkers (2016). Locations indexed by 1-18 are short tidal lagoons (L is the length of the flood basin), while the rest 19-39 are estuaries (L_b is the convergence length). The reader is referred to the main text for the meaning of parameters. The name of locations is indicated by two capital letters (shown in the colume of Index/Identifier) which may be used in Figure 9.

Index/ Identifier	Data location	$\frac{a}{h}$	$\frac{B_{HW}-B_{LW}}{B_{HW}+B_{LW}}$	L or L_b (km)	$2a$ (m)	h (m)	Δt_{FR}^{mouth} (hour)
1-ES	Eastern Scheldt	0.115	0.130	40	3.0	13.0	0.1
2-TE	Texel Inlet	0.097	0.091	50	1.5	7.7	0.6
3-EI	Eijerland Inlet	0.236	0.474	12	1.7	3.6	0.5
4-VL	Vlie Inlet	0.158	0.259	25	1.9	6.0	0.4
5-AM	Ameland Inlet	0.164	0.333	22	2.1	6.4	0.6
6-FR	Frysian Inlet	0.169	0.375	20	2.3	6.8	0.2
7-LA	Lauwers Inlet	0.180	0.429	17	2.3	6.4	0.4
8-ED	Ems-Dollard	0.169	0.375	20	3.0	8.9	0.3
9-OB	Otzumer Balje	0.269	0.500	10	2.8	5.2	0.3
10-LD	Lister Dyb	0.180	0.333	20	1.8	5.0	1.2
11-LH	Langstone Harbour	0.428	0.600	5	3.25	3.8	–1.4
12-BA	Bassin Arcachon	0.288	0.200	15	3.0	5.2	–0.2
13-WA	Wachapreague	0.295	0.444	10	1.3	2.2	0
14-MM	Murrells Main Creek	0.348	0.556	7	1.6	2.3	1.0
15-MO	Murrells Oaks Creek	0.533	0.600	4	1.6	1.5	1.0
16-NO	North Inlet	0.375	0.556	6.5	1.5	2.0	0
17-WB	Willapa Bay	0.120	0.286	32	3.0	12.5	–0.6
18-MU	Mussolo Bay	0.130	0.375	26	1.2	4.6	0
19-WS	Western Scheldt	0.119	0.130	45	3.8	16	0.25
20-SC	Scheldt	0.265	0.048	21	5.3	10	0.75
21-TH	Thames	0.192	0.310	20	4.6	12	0.55
22-HB	Humber	0.233	0.167	30	5.6	12	0
23-DE	Dee	0.333	0.500	10	6.0	9	1.2
24-DY	Dyfi	0.327	0.600	6.5	3.6	5.5	1.5
25-RI	Ribble	0.375	0.600	6	6.0	8	0.6
26-EL	Elbe	0.138	0.091	40	3.3	12	0.9
27-WE	Weser	0.222	0.130	22	4.0	9	0.3
28-EM	Ems	0.254	0.000	22	3.3	6.5	0.6
29-SE	Seine	0.344	0.000	25	5.5	8	2.4
30-LO	Loire	0.281	0.048	23	4.5	8	1.6
31-CH	Charente	0.417	0.048	10	5.0	6	1.0
32-GI	Gironde	0.233	0.091	40	4.2	9	1.4
33-SA	Satilla R.	0.193	0.286	18	2.7	7	0.5
34-OR	Ord	0.429	0.333	15	6.0	7	0
35-HO	Hooghly	0.191	0.048	36	4.2	11	0.65
36-FL	Fly	0.200	0.048	40	4.0	10	0.1
37-SO	Soirap	0.260	0.091	22	2.6	5	0
38-GO	Gomso Bay	0.375	0.667	7.5	6.0	8	0.2
39-PU	Pungue	0.217	0.333	17	5.0	11.5	0.8

References

Aubrey, D. and Speer, P. (1985). A study of non-linear tidal propagation in shallow inlet/estuarine systems Part I: Observations. *Estuarine, Coastal and Shelf Science*, 21(2):185–205, doi:10.1016/0272-7714(85)90096-4.

Boon, J. and Byrne, R. (1981). On basin hyposmetry and the morphodynamic response of coastal inlet systems. *Mar. Geol.*, 40(1-2):27–48, doi:10.1016/0025-3227(81)90041-4.

Brown, J. and Davies, A. (2010). Flood/ebb tidal asymmetry in a shallow sandy estuary and the impact on net sand transport. *Geomorphology*, 114(3):431–439.

Cai, H., Savenije, H. H., and Toffolon, M. (2012). A new analytical framework for assessing the effect of sea-level rise and dredging on tidal damping in estuaries. *Journal of Geophysical Research: Oceans*, 117(C9), doi:10.1029/2012JC008000.

D'Alpaos, A., Lanzoni, S., Marani, M., and Rinaldo, A. (2010). On the tidal prism–channel area relations. *Journal of Geophysical Research: Earth Surface*, 115(F1), doi:10.1029/2008JF001243.

Dastgheib, A., Roelvink, J., and Wang, Z. (2008). Long-term process-based morphological modeling of the Marsdiep Tidal Basin. *Marine Geology*, 256(1-4):90–100, doi:10.1016/j.margeo.2008.10.003.

Davies, G. and Woodroffe, C. D. (2010). Tidal estuary width convergence: theory and form in North Australian estuaries. *Earth Surface Processes & Landforms*, 35(7):737–749, doi:10.1002/esp.1864.

Dissanayake, D., Ranasinghe, R., and Roelvink, J. (2012). The morphological response of large tidal inlet/basin systems to relative sea level rise. *Clim. Change*, 113(2):253–276.

Dronkers, J. (1986). Tidal asymmetry and estuarine morphology. *Netherlands Journal of Sea Research*, 20(2-3):117–131.

Dronkers, J. (1998). Morphodynamics of the Dutch Delta. In Dronkers and (eds), S., editors, *Proceedings of the 8th International Biennial Conference on Physics of Estuaries and Coastal Seas.*, pages 297–304, Rotterdam: Balkema.

Dronkers, J. (2005). *Dynamics of coastal systems*, volume 25 of *Advanced series on ocean engineering*. World Scientific, Singapore.

Dronkers, J. (2016). *Dynamics of coastal systems*, volume 41 of *Advanced series on ocean engineering*. World Scientific, Singapore, 2nd edition.

Friedrichs, C. (2010). Barotropic tides in channelized estuaries. In Valle-Levinson, A., editor, *Contemporary issues in estuarine physics.*, pages 27–61. Cambridge University Press: Cambridge.

Friedrichs, C. and Aubrey, D. (1988). Non-linear tidal distortion in shallow well-mixed estuaries: a synthesis. *Estuar. Coast. Shelf Sci.*, 27(5):521–545, doi:10.1016/0272-7714(88)90082-0.

Friedrichs, C. T. and Aubrey, D. G. (1994). Tidal propagation in strongly convergent channels. *J. Geophys. Res.*, 99:3321–3336.

Friedrichs, C. T., Aubrey, D. G., and Speer, P. (1990). Impacts of relative sea-level rise on evolution of shallow estuaries. In Cheng, R. T., editor, *Residual currents and long-term transport*, volume 38, pages 105–122. Springer, doi:10.1007/978-1-4613-9061-9_9.

Friedrichs, C. T. and Madsen, O. S. (1992). Nonlinear diffusion of the tidal signal in frictionally dominated embayments. *J. Geophys. Res.*, 97(C4):5637–5650, doi:10.1029/92JC00354.

Gao, S. and Collins, M. (1994). Tidal inlet equilibrium, in relation to cross-sectional area and sediment transport patterns. *Estuarine, Coastal and Shelf Science*, 38(2):157–172, doi:10.1006/ecss.1994.1010.

Geyer, W. R. and MacCready, P. (2014). The estuarine circulation. *Annual review of fluid mechanics*, 46:175–197, doi:10.1146/annurev-fluid-010313-141302.

Gong, W., Jia, L., Shen, J., and Liu, J. T. (2014). Sediment transport in response to changes in river discharge and tidal mixing in a funnel-shaped micro-tidal estuary. *Continental Shelf Research*, 76(2):89107, doi:10.1016/j.csr.2014.01.006.

Green, M. O. and Coco, G. (2014). Review of wave-driven sediment resuspension and transport in estuaries. *Reviews of Geophysics*, 52(1):77–117, doi:10.1002/2013RG000437.

Guo, L., van der Wegen, M., Roelvink, J. A., and He, Q. (2014). The role of river flow and tidal asymmetry on 1-d estuarine morphodynamics. *Journal of Geophysical Research: Earth Surface*, 119(11):2315–2334, doi:10.1002/2014JF003110.

Hunt, S., Bryan, K. R., Mullarney, J. C., and Pritchard, M. (2016). Observations of asymmetry in contrasting wave- and tidally-dominated environments within a mesotidal basin: implications for estuarine morphological evolution. *Earth Surface Processes & Landforms*, 41(15):2207–2222, doi:10.1002/esp.3985.

Jarrett, J. (1976). Tidal prism - inlet area relationships. Technical report, US Army Corps of Engineers, Waterway Experiment Station, Vicksburg, MS, USA.

Jewell, S. A., Walker, D. J., and Fortunato, A. B. (2012). Tidal asymmetry in a coastal lagoon subject to a mixed tidal regime. *Geomorphology*, 138(1):171–180, doi:10.1016/j.geomorph.2011.08.032.

Lanzoni, S. and Seminara, G. (2002). Long-term evolution and morphodynamic equilibrium of tidal channels. *Journal of Geophysical Research*, 107(C1):3001–3001, doi:10.1029/2000JC000468.

Nidzieko, N. J. (2010). Tidal asymmetry in estuaries with mixed semidiurnal/diurnal tides. *J. Geophys. Res.*, 115(C8):C08006, doi:10.1029/2009JC005864.

Nidzieko, N. J. and Ralston, D. K. (2012). Tidal asymmetry and velocity skew over tidal flats and shallow channels within a macrotidal river delta. *J. Geophys. Res.*, 117:C03001–C03001.

Parker, B. B. (1991). *TIDAL INTERACTIONS (REVIEW)*, chapter 13 The relative importance of the various nonlinear mecanisms in a wide range of tidal interactions, pages 237–268. John Wiley & Sons.

Ranasinghe, R. and Pattiaratchi, C. (2000). Tidal inlet velocity asymmetry in diurnal regimes. *Cont. Shelf Res.*, 20(17):2347–2366.

Roberts, W., Dearnaley, M., Baugh, J., Spearman, J., and Allen, R. (1998). The sediment regime of the stour and orwell estuaries. In J., D. and M.B.A.M., S., editors, *Physics of Estuaries and Coastal Seas, Balkema, Rotterdam*, pages 93–102.

Savenije, H. (2012). *Salinity and Tides in Alluvial Estuaries*. 2nd completely revised edition, www. salinityandtides.com edition.

Speer, P. and Aubrey, D. (1985). A study of non-linear tidal propagation in shallow inlet/estuarine systems Part II: Theory. *Estuar. Coast. Shelf Sci.*, 21(2):207–224, doi:10.1016/0272-7714(85)90097-6.

Toffolon, M. and Lanzoni, S. (2010). Morphological equilibrium of short channels dissecting the tidal flats of coastal lagoons. *Journal of Geophysical Research*, 115(F4):F04036, doi:10.1029/2010JF001673.

Toffolon, M. and Savenije, H. (2011). Revisiting linearized one-dimensional tidal propagation. *J. Geophys. Res.*, 116:C07007, doi:10.1029/2010JC006616.

Townend, I. (2005). An examination of empirical stability relationships for UK estuaries. *J. Coast. Res.*, 21(5):1042–1053, doi:10.2112/03-0066R.1.

Townend, I. (2012). The estimation of estuary dimensions using a simplified form model and the exogenous controls. *Earth Surface Processes and Landforms*, 37(15):1573–1583, doi:10.1002/esp.3256.

van der Wegen, M. (2013). Numerical modeling of the impact of sea level riseon tidal basin morphodynamics. *J. Geophys. Res. Earth Surf.*, 118, doi:10.1002/jgrf.20034.

van der Wegen, M. and Roelvink, J. A. (2008). Long-term morphodynamic evolution of a tidal embayment using a two-dimensional, process-based model. *J. Geophys. Res.*, 113:C03016, doi:10.1029/2006JC003983.

van der Wegen, M., Wang, Z. B., Savenije, H. H. G., and Roelvink, J. A. (2008). Long-term morphodynamic evolution and energy dissipation in a coastal plain, tidal embayment. *J. Geophys. Res.*, 113:F03001, doi:10.1029/2007JF000898.

van Maanen, B., Coco, G., and Bryan, K. (2011). A numerical model to simulate the formation and subsequent evolution of tidal channel networks. *Australian Journal of Civil Engineering*, 9(1):61–71.

van Maanen, B., Coco, G., and Bryan, K. (2013). Modelling the effects of tidal range and initial bathymetry on the morphological evolution of tidal embayments. *Geomorphology*, doi:10.1016/j.geomorph.2013.02.023.

van Rijn, L. C. (2011). Analytical and numerical analysis of tides and salinities in estuaries; part i: tidal wave propagation in convergent estuaries. *Ocean Dynamics*, 61(11):1719–1741, doi:10.1007/s10236-011-0453-0.

Wang, Z., Jeuken, C., and de Vriend, H. (1999). Tidal asymmetry and residual sediment transport in estuaries. Technical report, Delft Hydraulics (now Deltares), The Netherlands.

Wang, Z., Jeuken, M., Gerritsen, H., De Vriend, H., and Kornman, B. (2002). Morphology and asymmetry of the vertical tide in the Westerschelde estuary. *Cont. Shelf Res.*, 22(17):2599–2609, doi:10.1016/S0278-4343(02)00134-6.

Wang, Z. B. and Townend, I. H. (2012). Influence of the nodal tide on the morphological response of estuaries. *Marine Geology*, 291-294:73–82, doi:10.1016/j.margeo.2011.11.007.

Whitehouse, R. J. S. (2006). Review and formalisation of geomorphological concepts and approaches for estuaries. Joint Defra/EA Flood and Coastal Erosion Risk Management R&D Programme Report number: FD2116/TR2, Prepared by HR Wallingford, ABPmer and Prof Pethick. This report can be accessed freely via www.estuary-guide.net/pdfs/FD2116_TR2.pdf.

Winterwerp, H. and Wang, Z. (2013). Man-induced regime shifts in small estuaries – i: Theory. *Ocean Dynamics*, 63:1279–1292, doi:10.1007/s10236-013-0662-9.

Zhou, Z., Coco, G., Jiménez, M., Olabarrieta, M., van der Wegen, M., and Townend, I. (2014a). Morphodynamics of river-influenced back-barrier tidal basins: The role of landscape and hydrodynamic settings. *Water Resources Research*, 50(12):9514–9535, doi:10.1002/2014WR015891.

Zhou, Z., Coco, G., Townend, I., Olabarrieta, M., van der Wegen, M., Gong, Z., D'Alpaos, A., Gao, S., Jaffe, B., Gelfenbaum, G., He, Q., Wang, Y., Lanzoni, S., Wang, Z., Winterwerp, H., and Zhang, C. (2017). Is "Morphodynamic Equilibrium" an oxymoron. *Earth-Science Reviews*, 165:257–267, doi:10.1016/j.earscirev.2016.12.002.

Zhou, Z., Olabarrieta, M., Stefanon, L., D'Alpaos, A., Carniello, L., and Coco, G. (2014b). A comparative study of physical and numerical modeling of tidal network ontogeny. *Journal of Geophysical Research: Earth Surface*, 119(4):892–912, doi:10.1002/2014JF003092.